Design of a Permanent Magnet Motor and a Drive for Cranking Purposes.

by

Gita Pappu

Thesis submitted to the Faculty of the

Virginia Polytechnic Institute and State University

in partial fulfillment of the requirements for the degree of

Master of Science

in

Electrical Engineering

APPROVED:

Dr. Jaime De La Ree, Chairman

Dr. Arun G. Phadke

Dr. Saifur Rahman

August, 1989.

Blacksburg, Virginia

Design of a Permanent Magnet Motor and a Drive for Cranking Purposes.

by

Gita Pappu

Dr. Jaime De La Ree, Chairman

Electrical Engineering

(ABSTRACT)

The development of Magnaquench in 1985 by the Delco-Remy laboratories, increased the research of applications of permanent magnets for use in automobiles. However the application of permanent magnet machines for cranking purposes has not been investigated much.

Difficult operating conditions, like, a maximum current density of $35A/mm^2$, and the ability to withstand demagnetizing armature currents up to 250% of the stall current require a new design approach to be developed.

Commutation in the permanent magnet machine is obtained by a three phase full wave inverter. The machine - inverter model was simulated by a standard method (SPICE), and an second analytical method we developed.

A permanent magnet brushless motor and a drive for cranking purposes is designed and simulated as a part of this thesis.

Acknowledgements

First, I sincerely thank my advisor, Dr. Jaime De La Ree, for all the help and advise especially during some of my most trying times at Virginia Tech. My sincere thanks to Prof. Arun G. Phadke, and Prof. Saifur Rahman for being on my advisory committee. I am also grateful to Prof. Ramu Krishnan for all help he gave me during the course of my Graduate study.

My sincere thanks to the General Motors Research Laboratories, Electrical and Electronics department for sponsoring the project on which my thesis is based. I am especially grateful to Dr. Nady Boules, Electrical Engineering Department, GMRL, for his advise and help during the entire project.

I acknowledge with thanks the assistance I got from all my colleagues in the Power Systems Laboratory and outside. Thanks to Prof. Tront for the permission to use the VAX in the Computer Engineering Laboratory for the SPICE Simulation.

My sincere thanks to my family especially my parents, Mrs. Lakshmi Pappu and Mr. K. R. Pappu, for their continous support and encouragement throughout. Thanks to all

my friends who made my stay here at Blacksburg and my program at Virginia Tech a great experience.

Finally Navaneetha, thanks, for without your support things would have been a lot different and a lot less interesting.

Table of Contents

List of Illustrations

Introduction

The development of rare-earth cobalt magnets in the late sixties triggered the development of a number of new permanent magnetic materials, which in turn led to an increase in the applications of these new materials in rotating machines. Since the development of permanent magnets with large intrinsic coercivity and high remanent flux density, in the early seventies, research in permanent magnet machines has been progressing rapidly. Rare earth magnets have high coercive strengths (8000-9000 Oersteds) and also the ability to withstand demagnetization unlike earlier magnetic materials like Alnico which were prone to demagnetization. This allowed a large number of permanent magnet machines to be designed. Since the development of Magnaquench, coercivity of approximately 10,400 Oersteds, by Delco-Remy in 1985, the use of permanent magnets in automotive applications is increasing steadily. However, one of the applications where PM brushless machines are not commonly used is as a starter motor.

A number of electrical machines with high power to weight ratios have been designed with the new permanent magnet materials for low and and medium power levels (17, 25, 8). The factors which determine the choice of the magnetic materials are performance

and cost. Ferrite magnets have low coercivity and are generally used for drives where cost is a more important than performance. Ferrites are also preferred in those applications where size is not a limiting constraint, because to obtain the flux required in the machine, the volume occupied by the Ferrite magnets will be considerable. Alnico has a high remanent flux density but a low coercivity, and is hence prone to demagnetization. Thus Alnico finds use in very small machines. For high performance, high power density motors, where cost is secondary to performance, rare earth magnets are used.

Advances in power-electronics also contributed to the rapid progress of AC drives. The increase in the performance and ratings of the various power electronic switches has allowed novel applications for these switches in high voltage/ high current drives. The availability of high current rating power transistors (200 amperes), has increased their application in low to medium power drives. The advent of MOSFETs, with their superior characteristics, on the scene is opening new avenues in converter technology. GTOs are being used in various low power machines.

Some of the advantages of PM brushless machines over the conventional machines are:

1. There are no windings on the rotor in a PM brushless machine unlike the conventional wound rotor machines. Thus, there are no copper losses associated with the rotor and the PM brushless machine is more efficient than the conventional machines.

2. The requirement of a mechanical commutator and a set of brushes in DC machines puts a limit on the maximum speed capability. The PM machines which are electronically commutated have no such limitations.

3. Sparking associated with the mechanical commutator makes the D.C. machine unsafe in certain environments but this is not a concern in the PM brushless machines.

4. Magnets in a PM brushless machine are much smaller in size than the conventional wound rotor of a synchronous machine or the field winding of a D.C. machine. Hence, for the same output a PM brushless machine will have a larger power density.

5. PM brushless machines have a higher efficiency because of the absence of copper losses in the rotor, absence of brush friction drop, and lower drop across the transistors compared to drop across the brushes.

6. There is a better heat dissipation in permanent magnet machines because the current runs in the stator, the outside armature winding.

7. The PM brushless machine has a low rotor inertia and a much simpler rotor construction.

However the PM brushless motors used for cranking purposes have some disadvantages also:

1. The inverter circuit increases the overall complexity of the whole system.

2. Additional requirement of rotor position sensors for accurate gating pulses.

There are two different types of constructions possible in the permanent magnet machines. The first is the buried rotor machine, and the second is the surface mounted magnet machine. The interior or buried magnets are used for flux concentrating.

Some of the differences in the surface mounted and buried magnet constructions are:

1. Interior magnet motors have a more complex rotor structure and construction compared to the surface mounted machines.

2. The buried magnet machines are like salient pole synchronous machines where the reluctance in the direct axis is different from the reluctance in the quadrature axis. The surface mounted machine is a non-salient pole machine.

3. Higher speeds are possible in the interior magnet constructions because the magnets are capable of withstanding much larger centrifugal forces.

4. The interior magnets, which may be rectangular, need no accurate shaping, unlike the surface mounted magnets which need accurate magnet shaping.

The cheaper, less complicated surface mounted magnet construction has been adopted in the design of the cranking motor. A number of papers on the analysis and design of surface mounted machines have appeared in literature (1, 11, 16, 22). This construction also yields a design with a smaller diameter (4). There is an upper limit on the maximum speed allowable on these machines and the magnets need special provisions to retain against centrifugal forces at higher speeds. The low electric conductivity of most permanent magnet materials reduces the harmonic content caused by non-sinusoidal components in the input waveform, in the surface mounted construction. This reduces the losses in the permanent magnet machine (5).

The question of designing a permanent magnet brushless drive for cranking purposes has been addressed in this thesis. The machine inverter model has been simulated using SPICE. An analytical model simulating the machine-inverter model was also developed.

Literature review

There has not been much published on the actual design of permanent magnet brushless motors. Weschta considers the procedure involved in the design of a permanent magnet servo-motor (25) and Pfaff (20) uses a similar procedure for designing brushless AC servomotors. Different motor designs for different input waveforms have been reviewed by Weschta in (25). Optimization of the magnet volume for obtaining low moment of inertia and similar design aspects have been discussed by Pfaff in (20). An empirical approach to machine design can be obtained from (13). The design of a DC motor for cranking purposes has been outlined by Patel (19). He has also discussed the effect of varying various design parameters like the number of poles, the maximum current density, input voltage, etc. on the main dimensions of the motor. The optimization of a permanent magnet DC motor based on its weight, size, cost, and efficiency was done by Boules (2). There have been quite a few reports on the analysis of the permanent magnet machines. The two dimensional field analysis of the surface mounted permanent magnet machines was done by Boules (2). There, both the lumped parameter approach as well as the current sheet representation approach of the magnetic excitation were studied. The torque produced in a permanent magnet synchronous motor and the cogging torque calculations in permanent magnet machines have been done in (6, 7). Jahns (11) investigated the torque production characteristics in a permanent magnet surface mounted

synchronous motor drive with rectangular current excitation, methods for reducing the low-speed pulsating torque have also been discussed in this paper.

Considerable attention has been paid to the dynamic modeling of the machine-inverter model. Novatny and Fath (18) used the digital computer to solve the steady state performance of a SCR single phase capacitor run induction motor. The excellent correlation obtained between the simulated waveforms and the waveforms from experiments proved the advantage the digital computer approach had over the analog approach. Since then the simulation of various drives has been investigated (12, 14, 15). Models for permanent magnet synchronous motors fed from a voltage source inverter (9) and a current source inverter (23) were developed from the analytical models developed by Slemon (24). A detailed numerical model of a permanent magnet brushless DC machine and the power electronic inverter for an electromechanical actuator, and an electric vehicle propulsion unit was presented by Nehl (17). Another detailed comparison between the permanent magnet brushless machine and a permanent magnet synchronous machine was presented by Pillay in (21). The power density, torque to inertia ratio, losses, thermal capability, and rectifier/inverter ratings were some of the characteristics compared.

Characteristics of the cranking motor

The availability of the present gear ratio of 40:1 allows the cranking motor to have a no-load speed of 7000 RPM. At such high speeds the motor size can be substantially smaller than the wound rotor machines. The magnetic material considered was

Magnaquench developed by Delco-Remy in 1985. The cranking motor designed has the following characteristics and constraints:

1. Output of 1.6 KW at a full load speed of 6500 RPM.

2. Maximum armature current density of 35 amperes per mm^2

3. Magnets should be able to withstand a current of 250 % of the stall current at -20°C.

Design Procedure

In general the output equation relates the main dimensions, and the electrical and magnetic loadings to the output power. In the conventional design procedure this equation may be written as:

$$S = C_1 D^2 L \qquad [1.1]$$

where C_1, the output constant, depends on both the magnetic loading, in Tesla, and the electrical loading, in A/m. D and L are the inside diameter and axial length of the stator and the rotor, respectively.

In the case of the problem given the electrical loading specified was in A/m^2 rather than in A/m thus requiring a new design procedure to be developed.

This relationship can be represented as:

$$S = C_0 D^3 L \qquad [1.2]$$

where C_0 is the new output constant, D and L are the outside diameter of the stator and the axial length of the rotor respectively.

This procedure is superior to the conventional design procedure because the output constant, C_0 , depends on the current density, the stator and slot dimensions, and the magnetic flux densities in various parts of the machine. Hence the design procedure from the very beginning conforms to the constraints set by the problem.

The basic assumptions made in the design procedure developed are the average flux density in the air-gap and the maximum allowable flux densities in the tooth cap and the yoke. These assumptions are valid because the density in the air-gap depends on the remanent flux density of the magnetic material. The flux densities in the tooth-cap and the yoke of the stator can be assumed taking into consideration the saturating flux densities of the stator material. The symbols used in the course of this thesis are explained in Appendix A. The flux densities in the air-gap, tooth, and core can be assumed to be:

$$B_g = (\frac{\pi}{2})\ \phi\ /(\pi\ D_{si}\ L/2p) \qquad [1.3a]$$

$$B_t = (\pi/2)\ /\phi\ (b_t\ N_s\ L/2p) \qquad [1.3b]$$

$$B_c = (\phi/2)\ /\ (b_i\ L) \qquad [1.3c]$$

These assumptions are later validated in Chapter IV using the following methods:

- WEMAP - Westinghouse Electromagnetic Analytical Package, and
- Analytical method developed by Boules & De La Ree.

Formulation of the Output Equation

The voltage induced in an AC machine depends on the flux per pole, ϕ , frequency, f, and the number of turns T_{ph}, and can be expressed as:

$$E = 4 K_f K_w \phi_m T_{ph} f \qquad [1.4]$$

The flux per pole can be expressed in terms of the flux density and the main dimensions as:

$$\phi = (\pi D_{si} L/2p) \; B_g \qquad [1.5]$$

Hence the induced EMF can be written as:

$$E = 4 K_f K_w T_{ph} f \; (D_{si} L/2 p) \; B_g \qquad [1.6]$$

The current density in a 3-phase AC machine, in terms of the number of phases, m, current, I, the number of slots, N_s, and the area of the copper in the machine, A_{cu} , can be expressed as:

$$J = \frac{2 m T_{ph} I}{N_s A_{cu}} \qquad [1.7]$$

The output in volt-amperes (VA) of an AC 3-phase machine can be written as:

$$S = E I \qquad [1.8]$$

Substituting for E and I from the [1.6] and [1.7] we obtain:

$$S = \frac{1}{m} K_f K_w \pi n B_g J N_s A_{cu} D_{si} L \qquad [1.9]$$

The output in terms of horse power can be expressed as:

$$HP = \frac{S \eta \cos(\phi)}{0.746} \qquad [1.10]$$

Considering the geometry of the machine Figure 1 on page 12 , the area of a rectangular slots can be represented, described by Honsinger (10) as :

$$A_s = \frac{h_1}{2}(w_{t1} + w_{t2}) + \frac{1}{2} h_2 (w_{t1} + b_0) + h_3 b_0 \qquad [1.11]$$

Assuming that the values of the slot opening b_o, height of the wedge h_2, and the height of the insulation h_3, are fixed the equation [1.11] can be simplified further. The main unknown dimensions in the slot are w_{t1}, w_{t2}, and h_1 .

The following equations relate the geometry of various dimensions in the machine. The first and the second relate the inside diameter and the outside diameter of the stator to the slot dimensions. The third equation relates the slot dimensions and the inside diameter of the stator to the outside diameter of the stator. The fourth and the final equation relate the tooth and the yoke dimensions to the flux densities.

$$\pi [D_{si} + 2 (h_2 + h_3)] = (w_{t1} + b_t) N_s \qquad [1.12]$$

$$\pi [D_{so} - 2 b_i] = (w_{t2} + b_t) N_s \qquad [1.13]$$

$$D_{so} = D_{si} + 2 (h_i + h_1 + h_2 + h_3) \qquad [1.14]$$

Permanent Magnet Synchronous Machine Cross Section

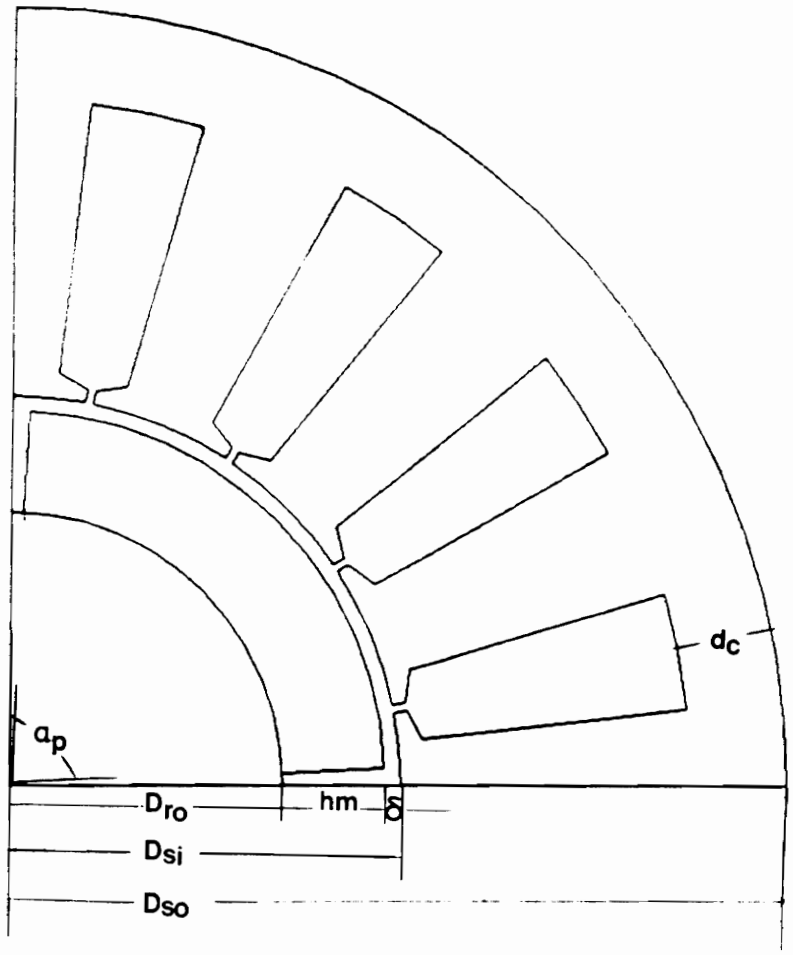

Figure 1. Cross - Section of the Permanent Magnet Machine

$$b_t = \frac{\pi \; D_{si} \; B_g}{N_s \; B_t} \qquad [1.15]$$

$$b_i = \frac{D_{si} \; B_g}{2p \; B_t} \qquad [1.16]$$

Solving the eq [1.12 - 1.16] we can obtain the values of the main unknowns in the slot dimensions, w_{t1} , w_{t2} , and h_1 as:

$$w_{t1} = \frac{\pi}{N_s} [\; D_{si} \; (1 - \frac{B_g}{B_t}) + c_k \;] \qquad [1.17]$$

$$w_{t2} = \frac{\pi}{N_s} [\; D_{so} - D_{si} (\frac{B_g}{pB_c} + \frac{b_g}{B_t}) \;] \qquad [1.18]$$

$$h_1 = (\; w_{t1} - w_{t2} \;) / (\frac{N_s}{2} \pi \;) \qquad [1.19]$$

The ratio of the copper area in each slot to the slot area for a round wire can be expressed as:

$$k_{cu} = \frac{A_{cu}}{A_s} = [(\pi / 4) \; d_{cu}^2 \, N_c] \; / \; A_s \qquad [1.20]$$

Substituting into the equation [1.11] the equation [1.17], [1.18], and [1.18] and substituting the result into the equation [1.20] the area of the slot can be expressed as:

$$a \; D_{si}^2 - 2 \, b \; D_{si} \, D_{so} + D_{so}^2 = (A_{cu} / k_{cu}) \; (4 \, N_s / \pi) \qquad [1.21]$$

where

$$a = (B_{gt} + B_{gc})^2 - (1 - G_{gt})^2$$

$$b = B_{gt} + B_{gc}$$

$$G_{gt} = B_g / B_t$$

$$G_{gc} = B_g - p\, B_c$$

In these calculations the second order terms of the dimensions like h_2 , h_3, and b_0 and the product of these terms have been neglected. This is a valid assumption because these dimensions are themselves very small and their products are small enough to be neglected.

Honsinger has presented a design procedure and optimization based on the volume of copper used to the volume of iron used (10). Since one of the most important considerations in optimizing the dimensions of the machine is its cost, it was decided that the procedure used in (10) be followed. Equation [1.21] can be rearranged as:

$$a \left[\frac{D_{sl}}{D_{so}} \right]^2 - 2\, b \frac{D_{si}}{D_{so}} + 1 = \frac{N_s A_{cu}}{\dfrac{(pi\, D_{so}^2)}{4\, K_{cu}}} \qquad [1.22]$$

If the ratio D_{si}/D_{so} is the optimizing function, λ, the eq [1.22] can be written as:

$$f_{cu}(\lambda) = a\lambda^2 - 2\, b\lambda + 1 \qquad [1.23]$$

From this the copper area can be obtained from equation [1.22] as:

$$A_{cu} = \frac{(\frac{\pi}{4} D_{so}^2)\ K_{cu}}{N_s} f_{cu}(\lambda) \qquad [1.24]$$

Substituting the value of A_{cu} into eq [1.9] the output equation may be rewritten as:

$$S = \frac{\pi^2}{4m} K_f K_w K_{cu} D_{sl} L B_g J D_{so}^2 f_{cu}(\lambda) \qquad [1.25]$$

Defining a function $f_o(\lambda)$ as :

$$f_o(\lambda) = \lambda f_{cu}(\lambda)$$

$$S = \frac{\pi^2}{4m} K_f K_w K_{cu} L B_g J D_{so}^3 f_o(\lambda) \qquad [1.26]$$

The optimizing function optimizes for the copper area in the machine. The values of the dimensions got may not be in the feasible region and hence a constant C_k is used as a multiplier to get feasible values for the main dimensions. Since the function $f_o(\lambda)$ is directly related to the size of the machine, the machine can be optimized based on the copper volume.

Hence the final output equation can be written as:

$$S = C_o D_{so}^3 L \qquad [1.27]$$

where the value of C_o is

$$C_o = \frac{\pi^2}{4m} K_f K_w K_{cu} B_g J f_o(\lambda) \qquad [1.28]$$

Separation of the Main dimensions

Once the value of the D^3L is got what remains is the separation of D and L. Usually there are design constraints on the either the length of the armature or the outer diameter of the machine. The larger the axial length of the machine the smaller will be the inner diameter of the stator, and hence smaller will be the volume. Hence for a more compact machine the ratio of L/D should be large. The weight and cost of the machine decreases with an increasing ratio of L/D. The inertia of the rotor is also inversely correlated to the ratio of L/D. This is an important consideration with servo-motors, and machines for machine control applications. However, a high L/D ratio means a large slot leakage and deeper slots. This in turn means a larger outside stator diameter. A machine with a large L/D ratio has poor ventilation and hence thermal considerations must also be taken into account when determining the ratio of L/D. Once the outside diameter is determined the effective axial length of the machine can be determined. The actual length of the machine is then to be calculated taking into account the possible need for air-ducts. Once the actual length of the machine is calculated the inside diameter of the stator can be calculated from the output equation.

Number of poles

Next, the number of poles is determined. The larger the number of poles, the smaller is the diameter of the machine, and hence smaller is the volume of the machine. However,

the number of poles is limited by iron losses and the cost of manufacturing. Generally in the permanent magnet applications the number of poles are limited to 4 or 6.

Once the number of poles has been determined the pole pitch, τ , can be calculated as:

$$\tau_p = \frac{\pi D_{si}}{2p} \qquad [1.29]$$

Number of slots

The number of slots is chosen next. The factor number of slots/pole/phase, q, can either be a whole number or a fraction. A fractional winding is adopted at times to reduce the torque ripple, mostly the ripple related to cogging or reluctance torque (7). Once the value of q is fixed the number of stator slots can be calculated from :

$$N_s = 2p\ m\ q \qquad [1.30]$$

Slot pitch

Next, the slot pitch is calculated from :

$$\tau_s = \frac{\pi D_{si}}{N_s} \qquad [1.31]$$

Slot geometry

The tooth and slot widths are determined, after the slot pitch has been calculated. The tooth width is determined generally by the saturating flux density in the tooth. Also there is a lower limit set on the tooth width, below which the tooth is not mechanically feasible. The tooth width is calculated as:

$$b_t = \frac{\pi D_{si}}{N_s} \frac{B_g}{B_t} \qquad [1.32]$$

Once b_t is known the width of the slot can be calculated. There are two possible configurations:

- The slot could have parallel sides, therefore, the tooth be trapezoidal.
- The tooth have parallel sides, therefore, the slot be trapezoidal.

In the former case, the width of the tooth must be calculated taking into consideration that the flux density at the narrowest part must be at B_{sat}. The latter configuration has been used in designing the machine described in this thesis.

The slot opening can be of various configurations:

1. ***Open slots:*** This option produces a larger effective gap, therefore a larger magnet is required to obtain the necessary air-gap flux density.

2. ***Closed slots:*** For this option the effective air-gap may be small, but larger leakage and saturation at the tooth-tip make it unattractive.

3. ***Semi-closed slots:*** This design has properties inbetween the above two options.

Semi-closed slots were chosen in order to reduce the leakage flux in the air-gap. There is a torque ripple caused by the non-uniformity of the air-gap and the harmonics in the back EMF. The no-load torque ripple can be reduced by skewing of the slots, or by using a fractional number of slots/pole/phase as explained before. In the designed motor the slots were skewed by one slot pitch. That the skewing does not affect the back EMF to a great extent, can be seen from the Figure 2 on page 20 & Figure 3 on page 21. The skewing the slot pitch by one slot pitch reduced the third harmonic and the fifth harmonic content considerably. The width of the slot opening is chosen so as to facilitate ease in manufacture. Usually b_o is chosen to be about three times the conductor thickness.

The shape of the slot is shown in Figure 4 on page 22. The height of the slot is determined from the current density, number of turns per phase and the wire gage. The wedge thickness and the insulation thickness are chosen on the basis of experience. The insulation required depends on the particular application of the machine.

Slot dimensions

The tooth width is determined from the saturating flux density in the teeth. Once the tooth width is fixed, the width of the slot can be calculated. The slot height, h_s, can be calculated assuming the copper filling factor to be ranging from 0.3 for small machines with round wires to 0.5 for machines with wires with a square cross section. Thus, once the effective thickness of the wire being used and the number of conductors per slot are determined the area of the slot can be calculated. The width of the slot opening is as-

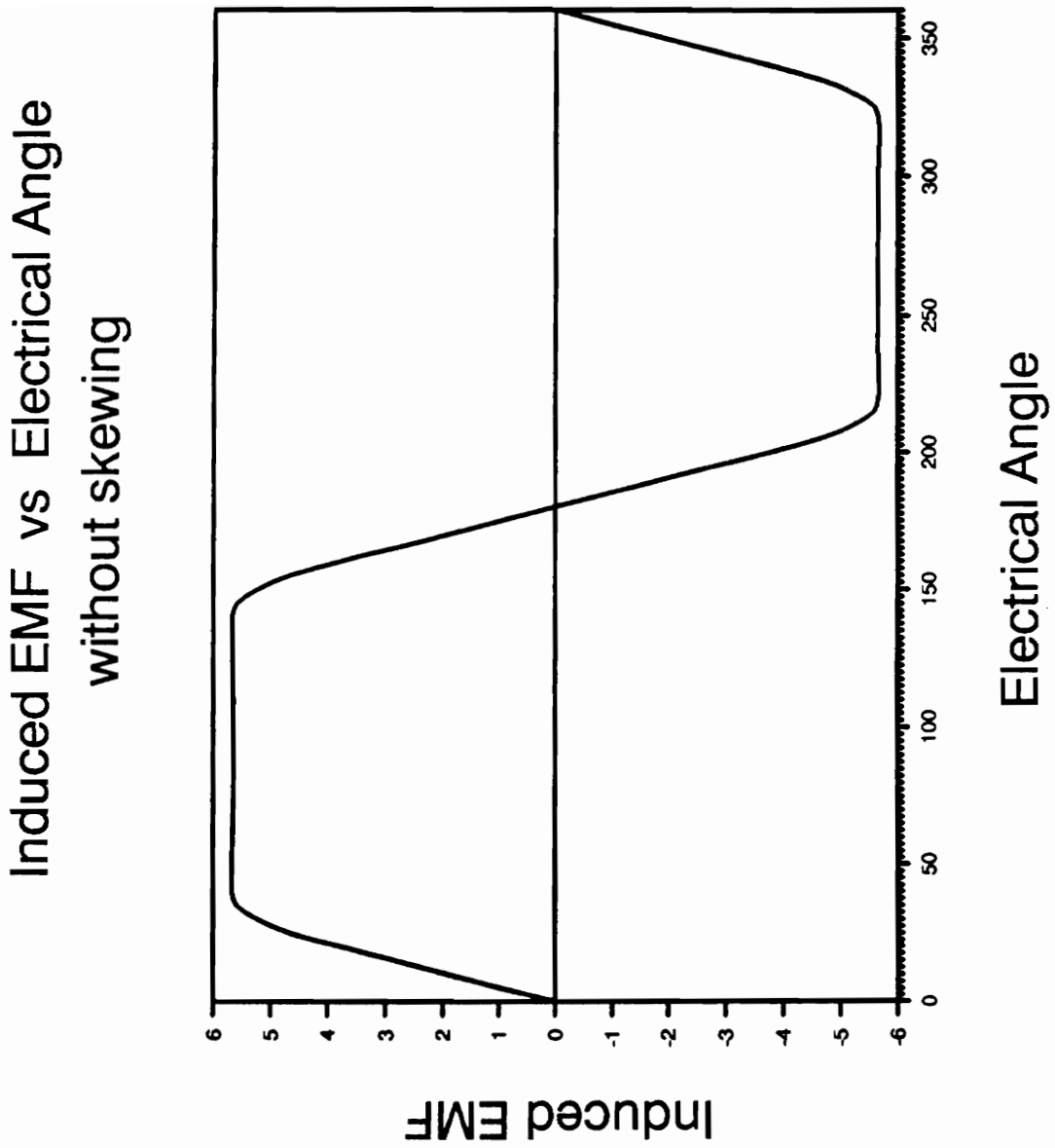

Figure 2. EMF vs Electric Angle without Skewing

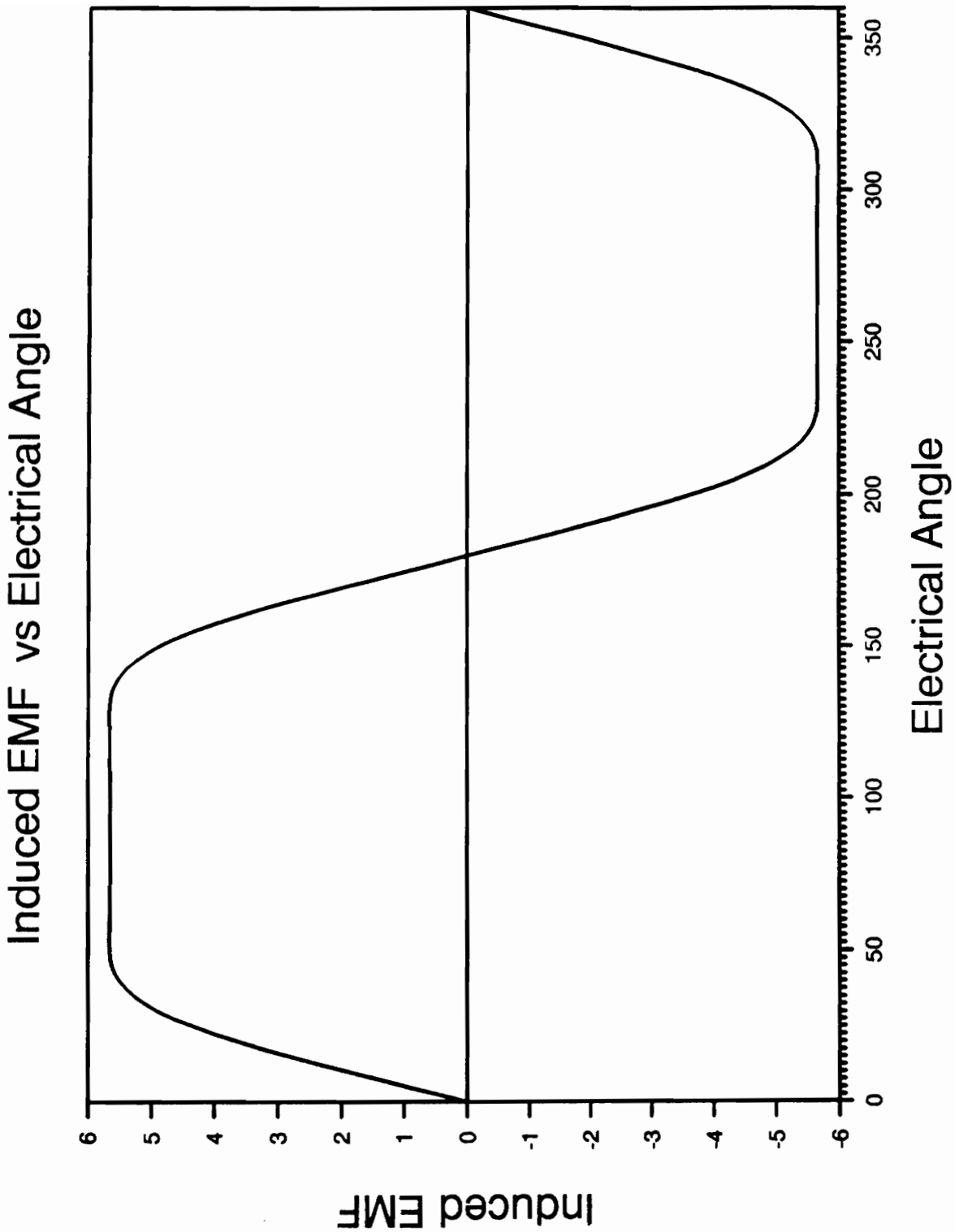

Figure 3. EMF vs Electric Angle with Skewing of one Slot Pitch

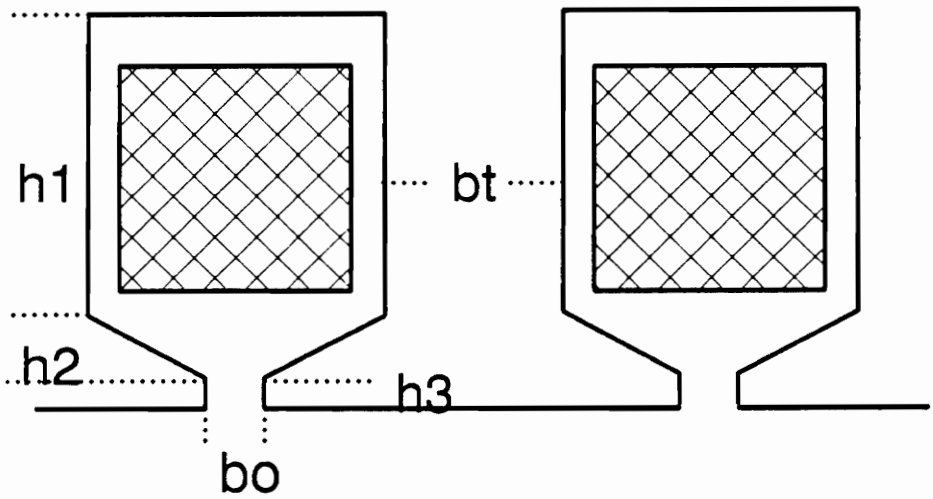

Figure 4. Slot Dimensions

sumed to about three times the diameter of the conductor, and in this case was assumed to be 0.03mm. The thickness of the wedge was assumed to be 0.08mm. This is assumed from previous available designs and experience.

Turns per phase

The number of turns per phase are calculated on the basis of the frequency, or the maximum speed. In general, n number of turns are connected in series to form the phase winding, each turn generating V volts, such that the sum gives the required Back EMF. The larger the number of turns, the larger will be the inductance. Also the higher the speed the larger will be the copper and iron losses. In order to avoid this the number of turns must be kept small. Hence, to ensure a low inductance for a machine with a good dynamic performance, and low iron and copper losses, the number of turns must be low, but large enough to generate the required back EMF. The effective number of turns can be expressed as:

$$N_{eff} = \frac{V_{ph}}{2\frac{\pi}{p} f_{\max} K_w L B_g D_{si}} \qquad [1.32]$$

To account for the distribution of the turns over the armature, rather than a concentrated set of turns, the actual number of turns can be calculated as:

$$T_{ph} = K_{dp} N_{eff} \qquad [1.33]$$

where K_{dp} is the product of the distribution factor ,the skewing factor, and the pitch factor. For a full pitch coil the pitch factor is 1. Hence, the effective number of turns can be written as:

$$T_{ph} = K_d N_{eff} \qquad [1.34]$$

Next, the number of conductors per slot are calculated as:

$$c_s = \frac{2mN_{ph}}{N_s} \qquad [1.35]$$

Now, the current sheet in the machine can be calculated. This may be used as a check since there is a maximum limit specified. The current sheet is:

$$J = \frac{3\sqrt{2}\ N_{ph}\ K_w\ I}{p\ \tau} \qquad [1.36]$$

Air-Gap Length

The physical length of the air gap is chosen based on the mechanical constraints. The smallest air gap which is mechanical feasible is chosen. The larger the air gap, the larger is the magnetizing current and hence poorer is the power-factor in wound field rotors, and larger the magnet in permanent magnet machines. To take into account the effect of the slot openings on the air-gap flux density, the Carter coefficient has to be taken into consideration. This is because the slot openings make the effective air-gap larger than the actual air-gap. The saturation factor accounts for the ampere turns required

to drive the magnet flux through the iron. Hence the effective air gap length can be written as:

$$g_{eff} = k_{sa}\ k_c\ \delta \qquad [1.37]$$

The Carter coefficient may be approximated as (13):

$k_c \sim 0.7S^{0.6}$

and the saturation factor may be approximated as:

$k_{sa} \sim 2.2S^{-0.05}$

Magnetic circuit design

As explained in Chapter I, one of the most important considerations in the design of the cranking motor is the design of the magnetic circuit. The magnet must be able to withstand the high demagnetizing armature currents especially at low temperatures. The magnetic material must be chosen such that it has linear characteristics in the second quadrant of the B-H curve. Thus the material must be chosen such that the operating point will always remain on the straight line as shown in the Figure 5 on page 26.

In order that the magnet be protected from demagnetization the B-H characteristics of the material must be accurately known. Typically, magnetic materials are characterized by their normal remanence, B_r , coercivity, H_c, and the intrinsic coercivity, H_{ci} , at room

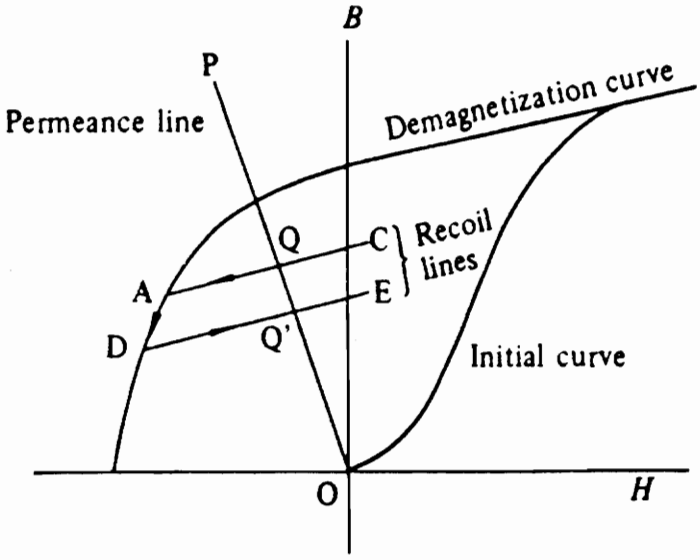

Figure 5. Magnetic characteristics important for demagnetization calulation

temperature. Some of the magnetic characteristics of some Permanent magnet materials are shown in Figure 6 on page 28.

Alnico magnets have a very high remanent flux density but a very low coercive force. Thus, Alnico is usually magnetized lengthwise.

Ferrite magnets, on the otherhand, have a low remanent flux density but a high coercivity. Furthermore, the low material and production costs allow ferrites to be used in applications where cost, rather than the volume is an important consideration.

Samarium-cobalt magnet: This is a rare-earth magnet which has both a high remanent flux density and a large coercivity. Inspite of its high initial cost this material finds use, in machines with short axial lengths as a result of its mouldability and machinability. Hence ferrite magnets are used for low cost machines, and samarium-cobalt magnets where the cost can be justified.

Magnaquench: (Figure 7 on page 29) Developed by Delco-Remy in 1985 this magnetic material has a remanent flux density of 1.2 Tesla and coercivity of 10.4 kOe. As seen from the magnetic characteristics in the second quadrant the knee of the B-H curve is very low and hence the material can withstand large demagnetizing forces.

As seen from the B-H characteristics Figure 5 on page 26, under no circumstances should the magnetic flux density fall below the knee, that is below Bmin, to prevent demagnetization.

The magnetic characteristics which are of importance for the design of the magnetic circuit are:

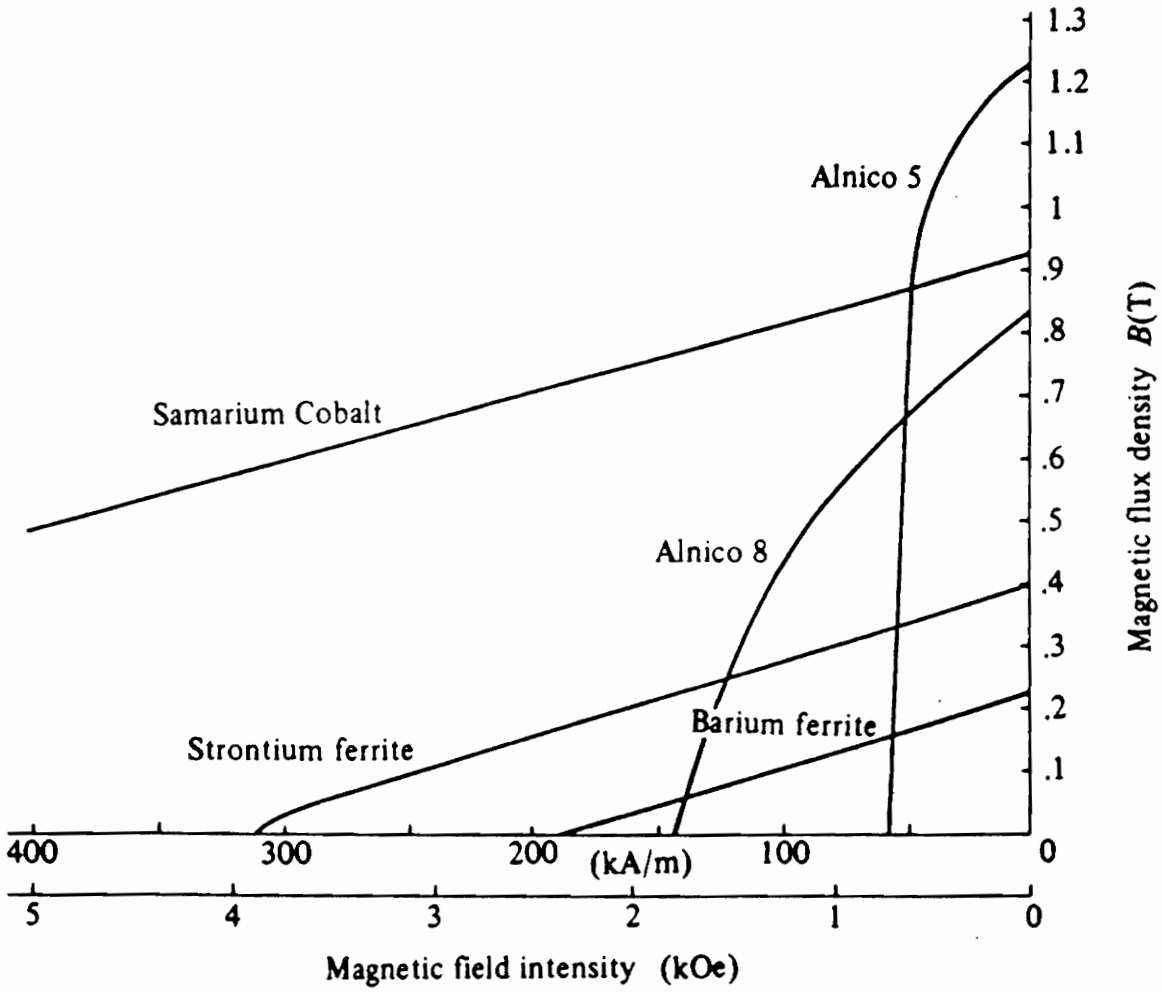

Figure 6. B - H Characteristics of some Permanent Magnet Materials

MQ III Temperature Characteristics (Normal)

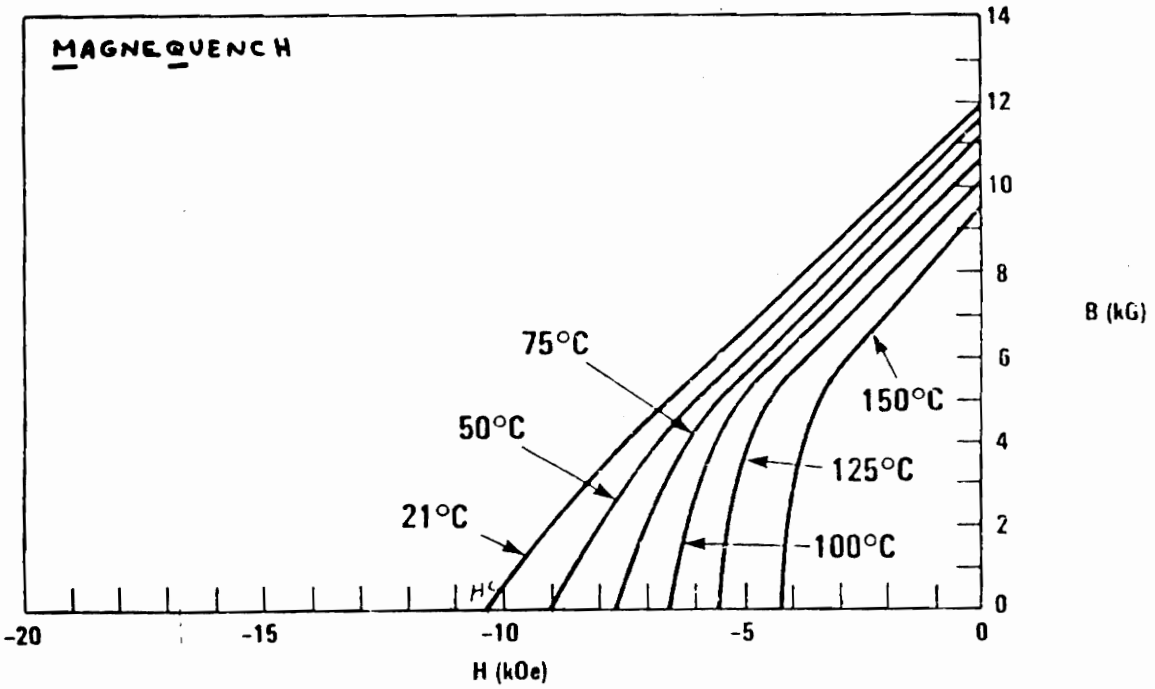

Figure 7. B - H Characteristics of Magnaquench III

1. Permeance line: The negative slope of the permeance line, PQ, can be determined from the construction parameters of the machine and can be expressed as:

$$\tan(\alpha) = \frac{h_m}{\delta} \mu_o \frac{A_g}{A_m} (1 + \alpha) \qquad [1.38]$$

2. Recoil lines: The minor loop in the second quadrant of the hystersis loop may be approximated by a straight line, called the recoil line. The recoil lines, AB & CD are as shown in the Figure 5 on page 26.

At the intersection of the lines AB and PO, the B-H characteristics of the recoil line and the permeance are satisfied and this point forms a stable operating point.

Irreversible demagnetization can occur when there are large armature currents, the magnetic field at one end of the pole is strengthened and the other is weakened, as a result of which the operating point moves down the recoil line till it reaches the minor loop. When this occurs and after the armature current is decreased the operating point may move down along the recoil line, DC, and thus the remanent flux density is decreased. This process is known as demagnetization.

To avoid irreversible demagnetization care must be taken to see that B_m is always greater than $B_{min.}$. As long as the operating point is on the straight line segment this condition is met. If this condition is not met the height of the magnet must be increased for the condition to be met.

Magnet demagnetization

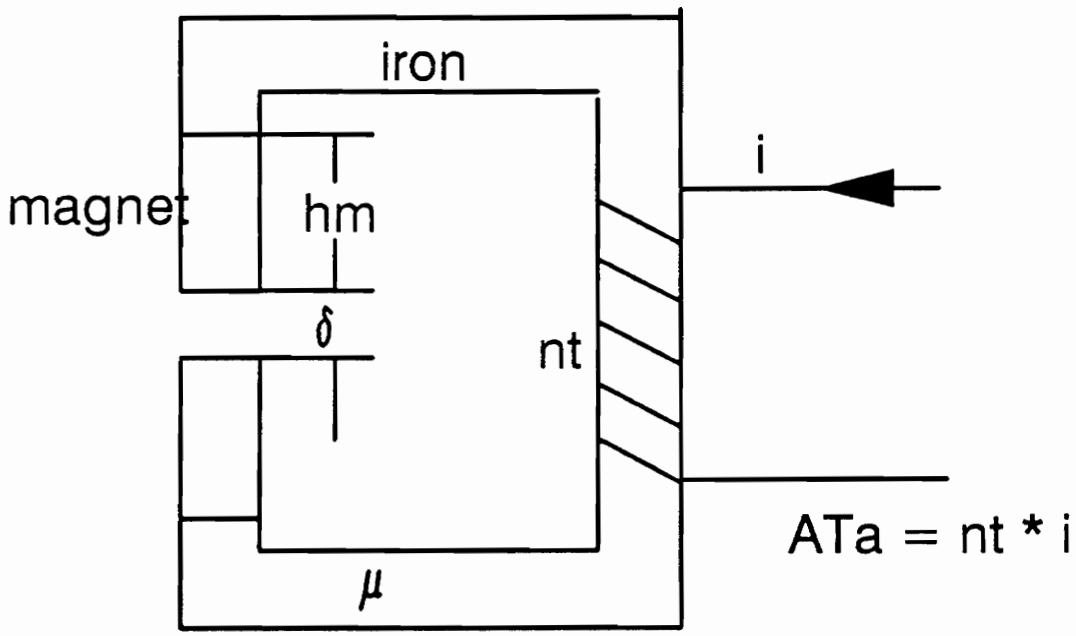

Figure 8.

To avoid demagnetization, $B_m > B_{\min}$ at all times. Using the lumped parameter approach (Figure 8 on page 31), the total number of ampere turns are,

$$(AT)_a = H_\delta \delta + H_m h_m \qquad [1.39]$$

$$H_\delta = \left[-\frac{H_m h_m}{\delta} + \frac{(AT)_a}{\delta} \right] \qquad [1.40]$$

$$B_m A_m = B_g A_g (1 + \sigma) \qquad [1.41]$$

$$B_m = \mu_o \frac{A_g}{A_m} (1 + \sigma) H_\delta \qquad [1.42]$$

From this the number of ampere turns can be expressed as:

$$(AT)_a = h_m\left[\frac{B_r}{\mu_m} - B_m\left[\frac{1}{\mu_o} + \frac{\delta}{h_m}\frac{A_m}{\mu_o A_g(1+\sigma)}\right]\right] \quad [1.43]$$

At maximum armature current, [1.43] can be expressed as:

$$(AT)_{\max} = h_m\left[\frac{B_r}{\mu_m} - B_{\min}\left[\frac{1}{\mu_o} + \frac{\delta}{h_m}\frac{A_m}{\mu_o A_g(1+\sigma)}\right]\right] \quad [1.44]$$

$B_{\min}$ depends on the magnetic material and is hence a known quantity. The maximum number of armature turns depends on the maximum allowable motor current, number of armature turns and the machine geometry, and can be calculated. The height of the magnet is a variable and must be adjusted such that at maximum armature demagnetization, the remanent flux density does not fall below $B_{\min}$

Resistance and Inductance calculations

The resistance of the armature winding must be calculated taking into account the length of overhang also. The length overhang can be assumed to be about 20% of the total length of winding. The resistance of the winding is :

$$R = \frac{2\ T_{ph}\ L_o}{\gamma\ q_o} \quad [1.44]$$

where L_o is the total length of the winding, q_o is the cross - section of the conductor, and γ is the conductivity of copper.

The leakage inductance consists of the following components:

- Slot inductance
- Tooth - cap inductance
- End winding or overhang inductance

The leakage inductance can be expressed as:

$$L_s = \mu_o \sum N^2 \lambda L \qquad [1.45]$$

Where λ is the permeance, which can be expressed as:

Permeance of the slot:

$$\lambda_s = \frac{h_1}{w_t} + \frac{2\,h_2}{w_t + b_o} + \frac{h_3}{b_o} \qquad [1.46]$$

Permeance of the tooth - top is:

$$\lambda_{tt} = \log_{10}\left(1 + \frac{\pi}{2}\frac{b_t}{b_o}\right) \qquad [1.47]$$

The permeance of the overhang can be expressed as:

$$\lambda_o = \frac{L_o}{L}\left[0.06 + 0.18 \log_{10} \frac{l_o}{b_p}\right] \qquad [1.48]$$

where b_p is the periphery of the conductor, and l_o is the length of the over - hang, which is assumed ass 0.2 L.

Inverter Design

This chapter deals with design of a suitable power electronic drive system for the cranking motor. The DC current must be first inverted to an quasi-square current AC and then fed to the PM Sync machine. Commutation is achieved using a three-phase full wave inverter circuit (Figure 9 on page 37) with six switches, the manipulation of which results in DC-AC inversion. Some of the advantages AC drives have over the DC drives are:

1. In an AC drive neither the power rating nor the maximum allowable speed is limited by the mechanical commutator, as in the case of a DC drive.

2. AC drives have a more rugged design and hence have less maintenance and service requirements.

3. AC drives have a better efficiency and occupy a smaller volume.

The synchronous motor drives have two different modes of operation. The first is the true synchronous mode of operation, where the speed is controlled by an independent

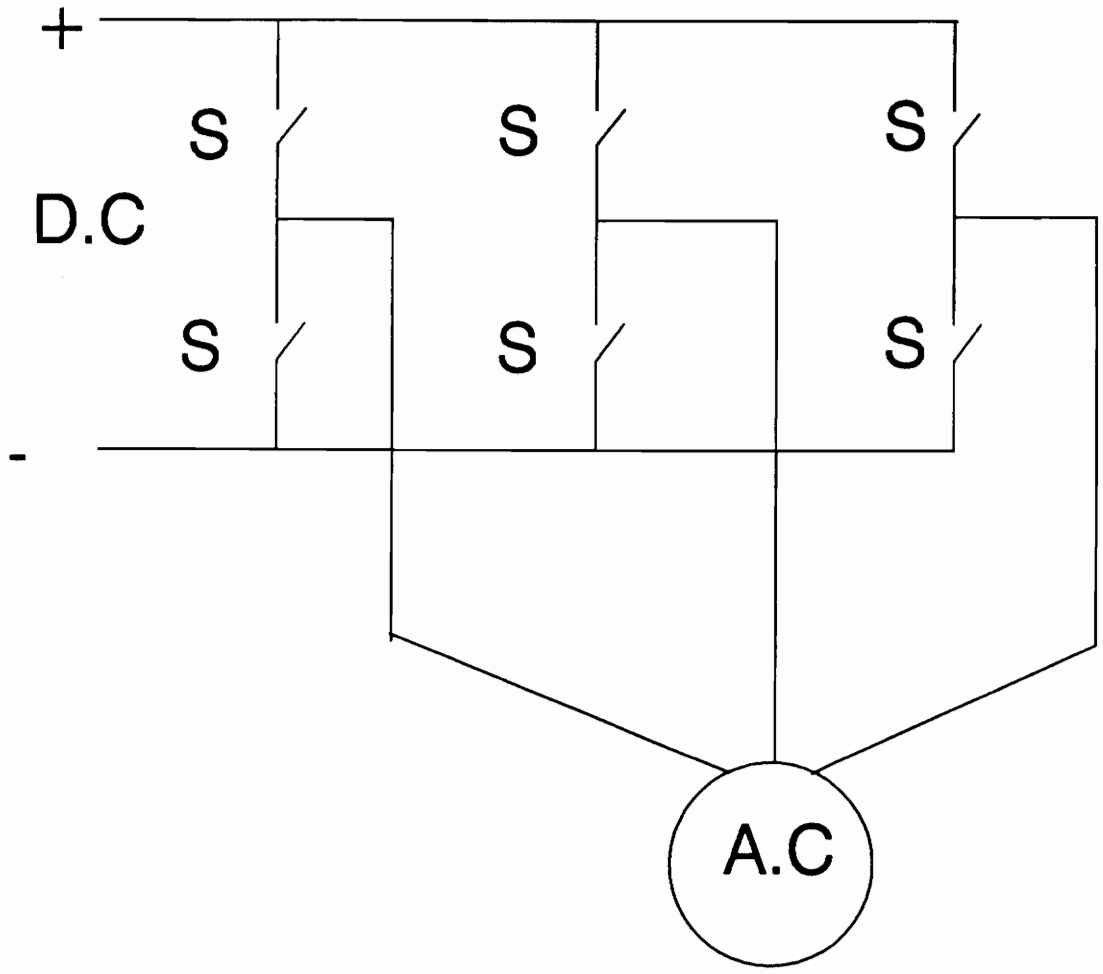

Figure 9. DC - AC Inverter Circuit

oscillator and the second mode of operation, electronically commutated mode (ECM), where the inverter firing signals are controlled by position sensors on the rotor. The two types of position sensors are (29) are:

1. Hall elements.

2. Light emitting diodes, photodiodes, or phototransistors (optical encoders).

Principle of operation of the Hall elements

The equivalent circuit of an Hall element is shown in Figure 10 on page 39. When the bias current, I_c, flows in the direction indicated, and a magnetic field, B, is present, then a voltage V_h is generated in a direction perpendicular to the current and the magnetic field as shown in Figure 10 on page 39. However the polarity of the voltage generated reverses if there is a reversal in the direction of the magnetic field. Thus, the Hall effect elements placed on the rotor surface can detect the pole position.

An example of how the Hall element detect the position and gives the firing pulses is shown in Figure 11 on page 41. As the Hall element detects the north pole of the rotor, a signal is given and the conductor, W_2 , is energized to produce a magnetic field such that the rotor rotates to position as shown in Figure 11 on page 41. In the figure it can be seen that no voltage is generated at the terminals of the Hall element and hence both the windings are not energized. However, rotor continues to rotate because of its inertia. Once the rotor approaches the position shown in Figure 11 on page 41 the Hall element detects a south pole and the winding W_2 is energized such that the rotor continues to rotate as before. This is the basic principle based on which the Hall elements on the

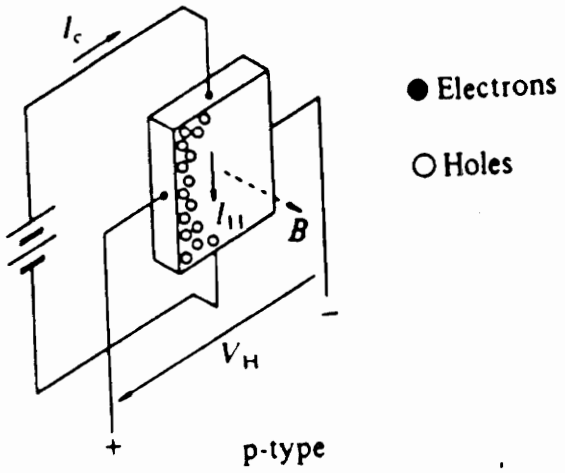

Figure 10. Rotor Sensor – Hall Element

rotor detect the position, and control the commutation in a permanent magnet brushless motor.

Principle of operation of the light sensitive devices

As shown in the Figure 12 on page 42, a three phase half wave rectifier needs three photosensitive devices. When one of the devices, say PT1, is exposed to the light, the transistor coupled to this is turned on. By repeating this action at the pre-calculated intervals the switching action in the permanent magnet motor can be achieved. For a three phase permanent magnet motor we require six photo transistors placed at equal intervals on the rotor.

The inverter may either be a voltage source or current source inverter. For this application a voltage source inverter is used because the inverter is being fed from a constant voltage battery. The stator interactions are directly controlled by the current controllers (Figure 9 on page 37). But care must be taken to ensure that the current does not go above the rated values. Also, the switch pattern must be so arranged that two switches on the same limb, as (T1,T4) ; (T3,T6) ;(T5,T2) are never conducting simultaneously, as this can short the battery. In case of starting or cranking motor a fixed frequency, non-variable speed drive is sufficient. Hence, a simple on-off voltage source inverter is used.

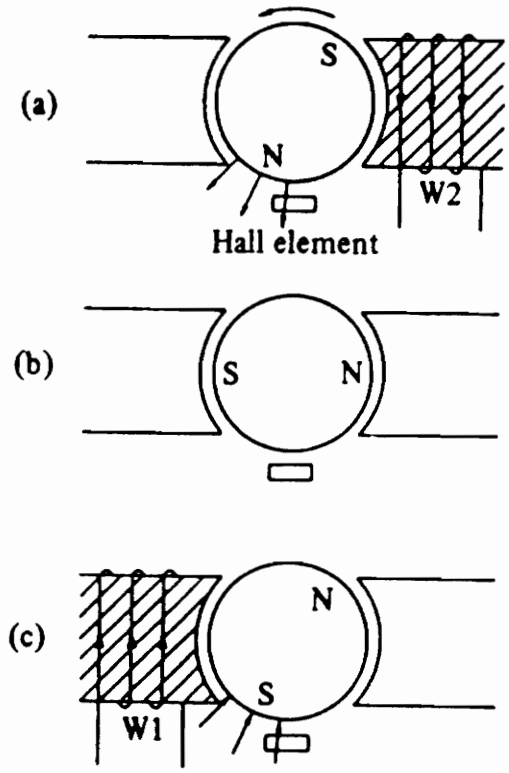

Figure 11. An example of switching with Hall effect devices

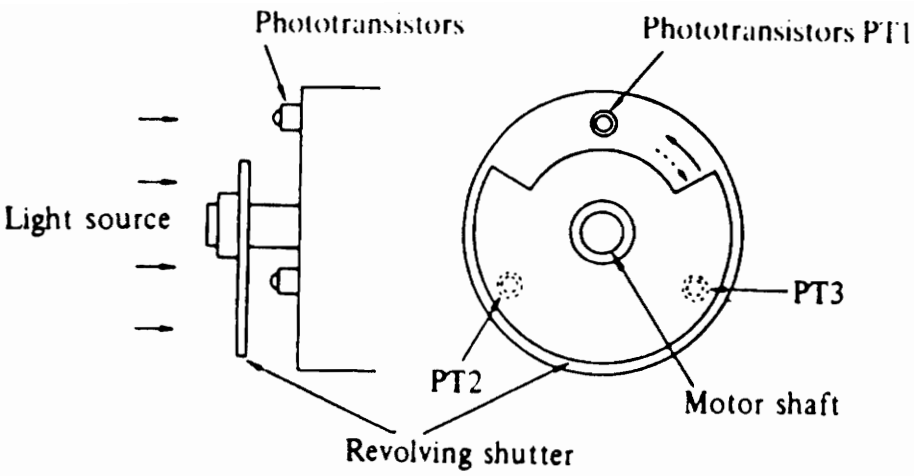

Figure 12. Rotor Position Sensor – Photosensitive Devices

Choice of Switches

Some of the semiconductor switches available are :

1. Silicon controlled Rectifiers (SCR/Thyristors).

2. Bipolar Junction Transistors (BJT).

3. Metal Oxide Field Effect Transistors (MOSFETS).

4. Gate Turn-off Devices (GTOS) etcetera.

Before the switch is selected, the ratings at which the switch is to be operated are considered. The switch must be able to handle currents up to 200 A continuous currents at 12 V. The switching frequency can be quite low. At such high currents, the devices available are:

- SCRs .

- BJTs and

- MOSFETs in parallel.

Comparison between transistors and thyristors

1. Switching Off: The transistor can be turned off by control of the base current, unlike a thyristor which can switched off by controlling its gate current after the main anode current is brought to zero by external means. This means that the thyristors have to be force commutated and hence need extra circuitry to achieve this. If these commutation circuits have capacitive elements there is an added energy loss in them.

2. Switching On: The thyristors being bi-stable devices need a relatively low pulse to be turned on. On the other hand the thyristors need a continuous and a substantial base current to be kept on. A Darlington may be used to increase the current gain, or reduce the base current requirements. This has the disadvantage of a higher Vce saturation which contributes to an increased power dissipation in the transistor.

3. Conduction losses: Within normal range of current, the voltage drop is less in a transistor.

4. Switching losses: Switching losses in both transistors and thyristors depend on the frequencies. Generally, switching-off losses are greater than the switching-on losses.

Hence BJT's are more advantageous than the SCR's for the application of a cranking motor. Recently MOSFETs have been replacing bipolars because of the several advantages they have over the BJTs :

- Ease in paralleling.

- Low conduction losses.
- Low gate drive requirements.
- High switching speeds, and
- Absence of secondary breakdown power restrictions.

One of the main disadvantages of the MOSFET's is the unavailability of these switches at the current ratings required. This will require the use of MOSFET's in parallel. This option is not economically viable when compared with bipolar switches for the same rating. Also at frequencies of operation, that is around 400 Hz, the high on-state losses in the MOSFET's favor the use of bipolars.

Configuration of the Inverter

A three phase full wave inverter as shown in the Figure 13 on page 47 with bipolars as the switching devices is used for commutating the cranking motor. These are represented by Q1, Q2 to Q6. The load current being generally inductive, stays practically constant during switch-off also. A freewheeling diode is required to divert the current during this time. The freewheeling diodes represented by FD1---FD6 are required to divert the current during this time. In power transistor circuits switching an inductive load during turn-on, the transistor is forced to switch from zero current to full load current before the voltage can fall from the the open circuit value. Similarly during

turn-off the voltage is forced to build up to its full value before the current can fall to zero. Assuming linear switching, the losses are:

$$W = \frac{E\,I\,t_s}{2} \qquad [2.1]$$

where $t_s = t_1 + t_2$, t_1 and t_2 being the rise time and fall time of the current respectively. I and E are the full load current and open circuit voltage. At current values under consideration these losses can be considerable. Hence, in power transistor circuits, snubber circuits are incorporated to reduce the switching losses and prevent reverse biased secondary breakdown. The two type of snubber circuits are:

- Turn-on snubber, and
- Turn-off snubber.

The turn-on losses could be eliminated by connecting a series inductor circuit for limiting the rate of rise of current in the switch. A turn-on snubber circuit can be seen in Figure 15 on page 49. Likewise, a capacitor in parallel with the switch can be used to limit the rise of voltage during turn-off (Figure 14 on page 48). There have been a number of articles on design of snubber circuits (26, 27, 28). Steyn (28) suggested the use of non-linear capacitors in the turn-off snubber circuits so as to optimize the snubber losses. Figure 16 on page 50 shows the complete inverter circuit.

MACHINE - INVERTER MODEL USED IN ANALYTICAL PROGRAM

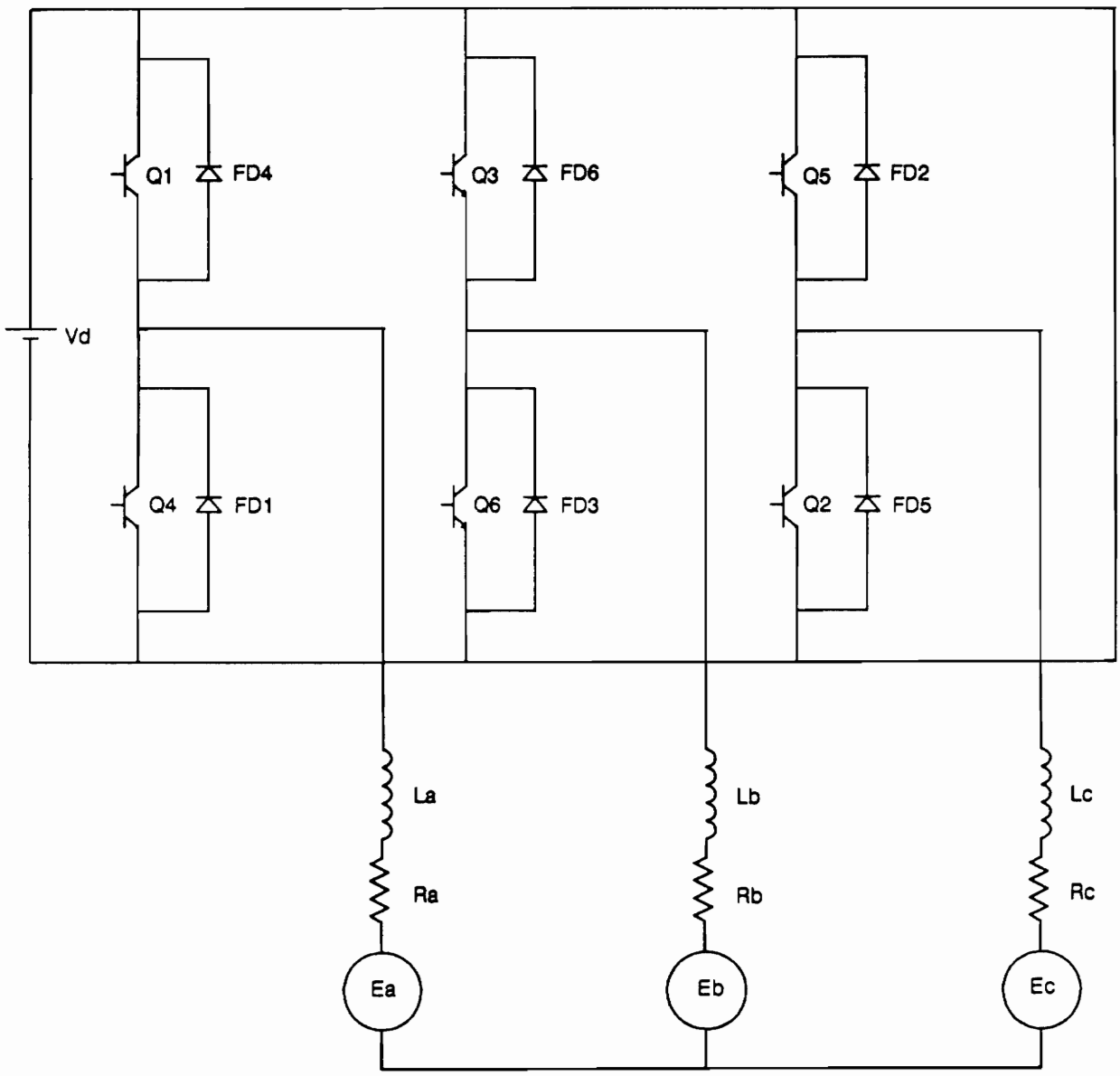

Figure 13. Basic Commutation Circuit

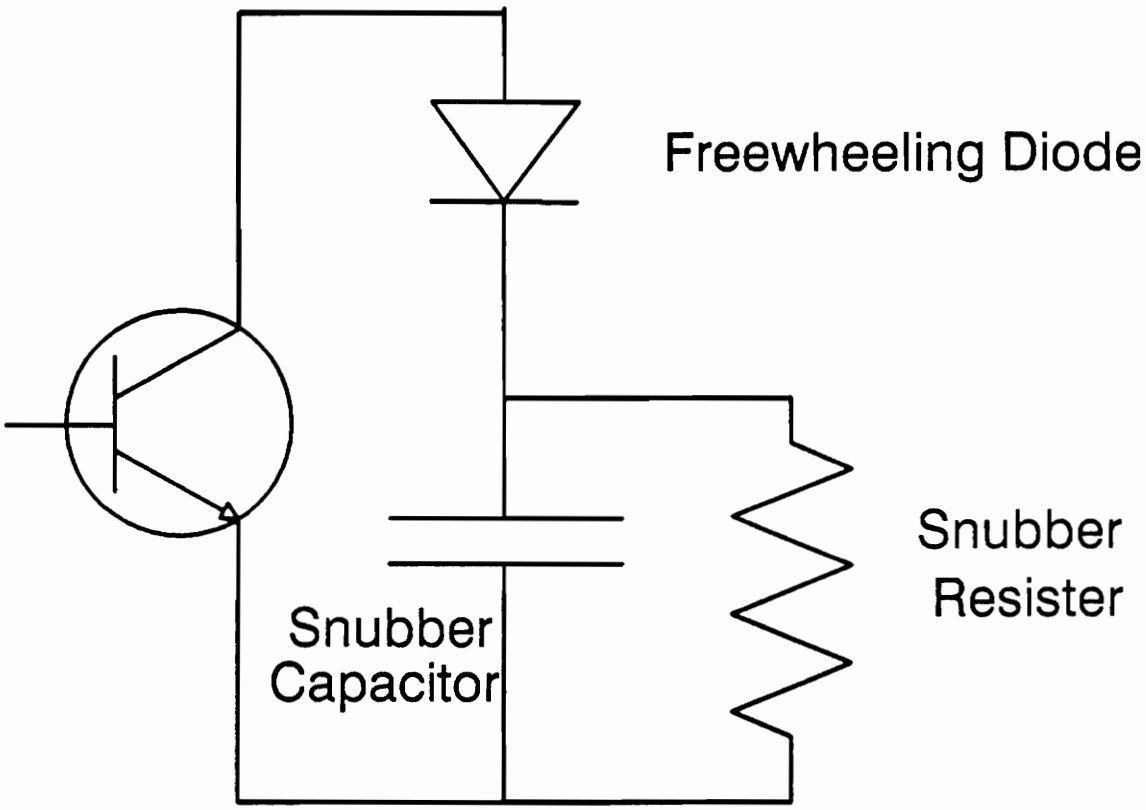

Figure 14. Turn - off Snubber Circuit

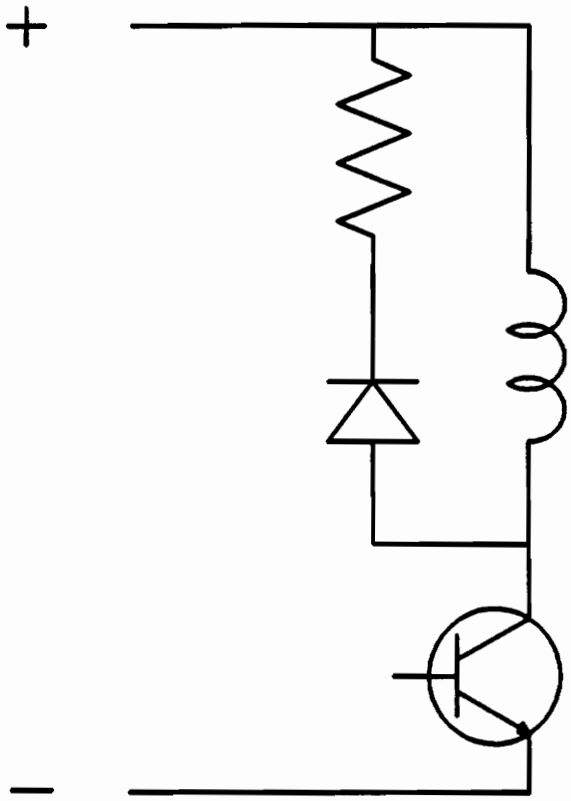

Figure 15. Turn - on Snubber Circuit

MACHINE - INVERTER MODEL USED IN SPICE

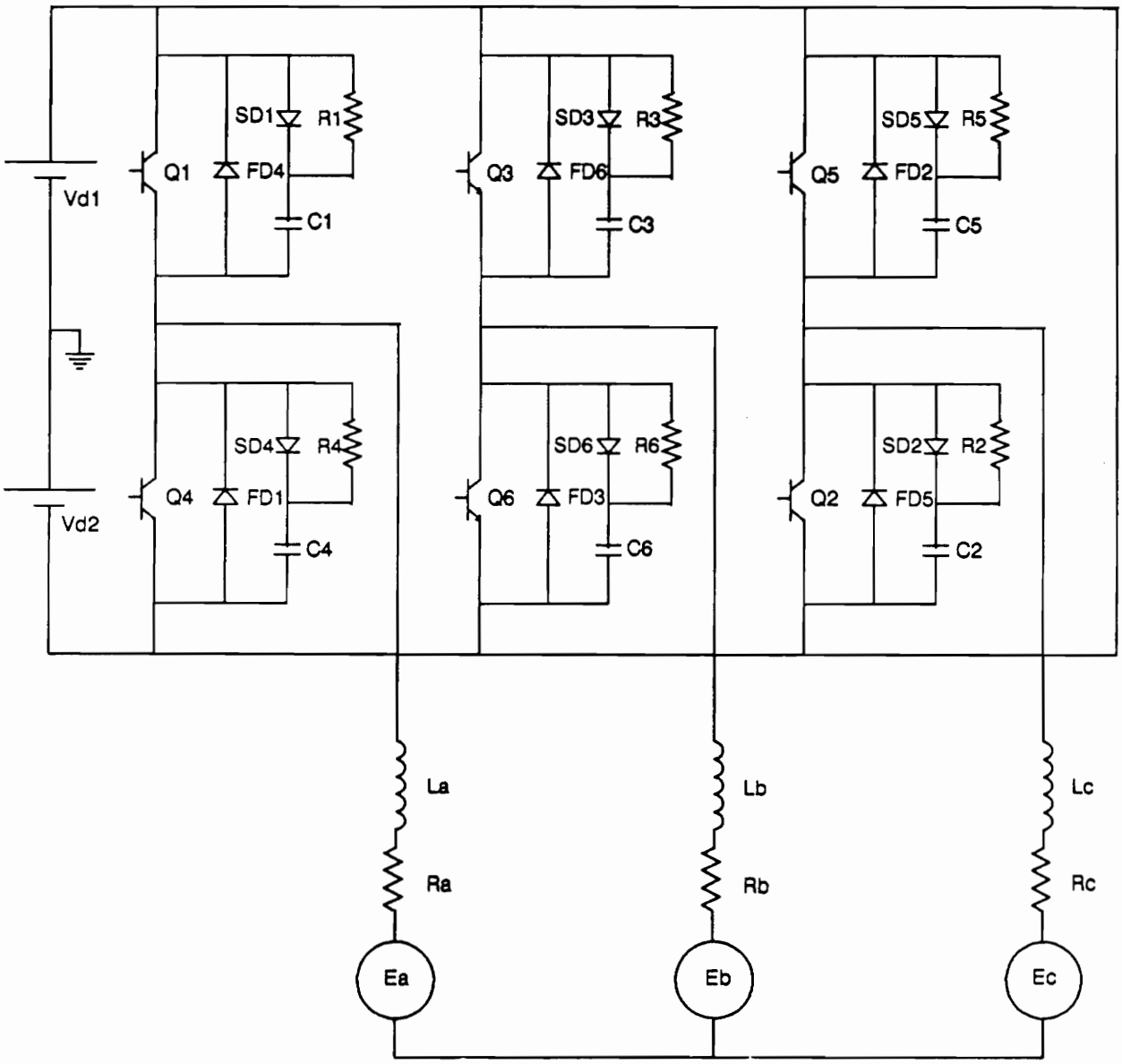

Figure 16. Complete Inverter - Machine Circuit

Ratings of the devices.

1. *Main Switches:*

The current ratings of the motor will determine the ratings of the transistors. The maximum overload current allowed should be taken into account because the transistors have a very low overload capacity and the devices must be designed to carry the maximum overload current continuously.

2. *Freewheeling Diodes:*

Freewheeling diodes in inductive circuits carry the full load current during turn-off. Hence these must be rated so as to carry the full rated current continuously. Especially, at low frequencies the freewheeling diode may have to carry the full load current for approximately 10ms -12ms and hence cannot be derated.

3. *Snubber Ratings:*

The turn-off snubber (Figure 14 on page 48) is made up of a capacitor in shunt with the switch which prevents the abrupt rise of voltage across the switch. The values of the capacitor and the resistor depend on the fall time of the switch and the ratings of the switch.

- Rating of the capacitor: If t_f is the fall time of the collector, that is the collector current falls from the full load value to zero in t_f secs, then the capacitor can be rated at:

$$C = \frac{I_{max}\ t_f}{2\ V_{in}} \qquad [2.2]$$

- Rating of the resistor: The rating of the resistor must be determined taking two points in consideration. First, the time needed for the capacitor to charge from V_{ce} to V_{in} through the resistor R, and secondly, the extra current needed from the source because of the shunt resistance. These two points contradict each other because the larger the value of the resistor the shorter will be the charging time but the extra current needed to be supplied by the source to the resistor is also larger. The value of the resistance used is calculated taking these two points into consideration as:

$$R = \frac{V_{in}}{I_{peak} - I} \qquad [2.3]$$

Where I_{peak} is the maximum continuous current rating of the transistor.

Analysis and Simulation of the Drive

WEMAP, The Westinghouse Electric and Magnetic field Analysis Program is a computer-aided engineering package for the analysis and design of electromagnetic components, devices, and systems. The software evaluates the thermal, magnetic, and electric designs. WEMAP is based on the finite element method (FEM), in which the region of interest is divided into a finite number of small interconnected elements. The FEM is based on the assumption that a region can be approximated or modelled by a finite number of individual elements. Hence the field variable, flux density in this case, which has infinite number of values in a region is reduced to a finite number of unknowns. The field variables at certain specified points, called nodes, are the approximating functions. These approximating functions define the conditions in each element. The nodal values of the field potentials form the unknowns, and interpolation of the field potentials define the potential in the elements as a whole.

First the whole region of interest is divided into a number of elements. Then the physical properties of each element, such as magnetic coercivity, permeability, conductivity of each element is defined and a matrix of differential equations formed. The boundary

conditions to these equations are then defined. The boundary conditions are either the Neumann boundary, where the normal derivatives are zero, or the Dirichlet boundary conditions, where the functional views are specified. The differential equations are solved either by the Gaussian Elimination if they are linear, or by the Newton-Raphson iterative method coupled with the conjugate gradient equation solver if they are non-linear.

The flux density which is the derivative of the magnetic potential is obtained as an output. The average flux density at any point, along any line, or arc can be obtained.

WEMAP was used to verify the assumptions made in the machine design procedure adopted in Chapter II. The assumption made was that the average flux density in the air-gap and the maximum flux densities in the tooth and yoke are known quantities. As seen from earlier (Appendix B) these were assumed to be:

- B_g = 0.96 Tesla
- B_t = 1.6 Tesla
- B_c = 1.4 Tesla

As seen from Figure 17 on page 56 the geometry of the machine, the open slot geometry was adopted. The semi-closed geometry was not generated as it was too complicated. The saturating effects and the slotting effects make the effective air-gap larger. The stator and the rotor are assumed to be made up of steel. The magnet is assumed to have a relative permeability of one. The magnetic properties defined are those of

Magnaquench III which has a remanent flux density of 1.2 T and an intrinsic coercivity of 10.4 KOe.

The magnetic flux density along the air-gap can be seen in Figure 18 on page 57. The average flux density in the air-gap is 0.955 T, which verifies the first assumption made. Figure 19 on page 58 gives the flux density along the radius of the machine. The maximum flux density in the stator is 1.1 T. This verifies the second and the third assumptions made. The no-load flux density distribution in the machine is shown in Figure 20 on page 59 .

Equivalent circuit of Permanent Magnet Motor

In general the three phase machines can be represented in a matrix form as (30):

$$\begin{bmatrix} v_a \\ v_b \\ v_c \\ v_f \end{bmatrix} = \begin{bmatrix} R_a & 0 & 0 & 0 \\ 0 & R_b & 0 & 0 \\ 0 & 0 & R_c & 0 \\ 0 & 0 & 0 & R_f \end{bmatrix} \begin{bmatrix} i_a \\ i_b \\ i_c \\ i_f \end{bmatrix} + p \begin{bmatrix} L_{aa} & L_{ab} & L_{ac} & L_{af} \\ L_{ba} & L_{bb} & L_{bc} & L_{fb} \\ L_{ca} & L_{cb} & L_{cc} & L_{fc} \\ L_{fa} & L_{fb} & L_{fc} & L_{ff} \end{bmatrix} \begin{bmatrix} i_a \\ i_b \\ i_c \\ i_f \end{bmatrix} \qquad [4.1]$$

where:

v_a, v_b, v_c, and v_f are the voltages in the phases A, B, C, and the field respectively.

i_a, i_b, i_c, and i_f are the currents in the phases A, B, C, and the field respectively.

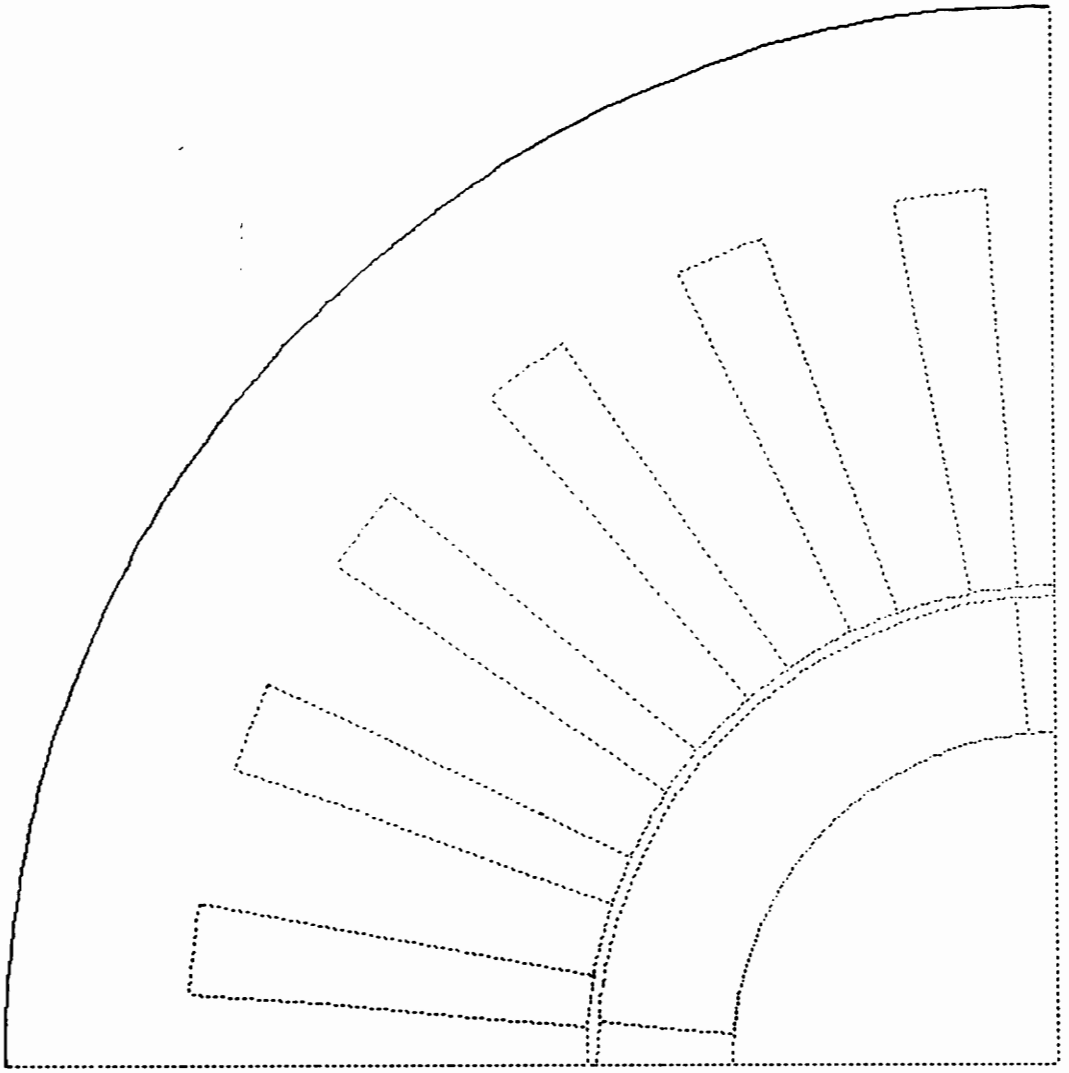

Figure 17. Cross Section of Machine Simulated on WEMAP

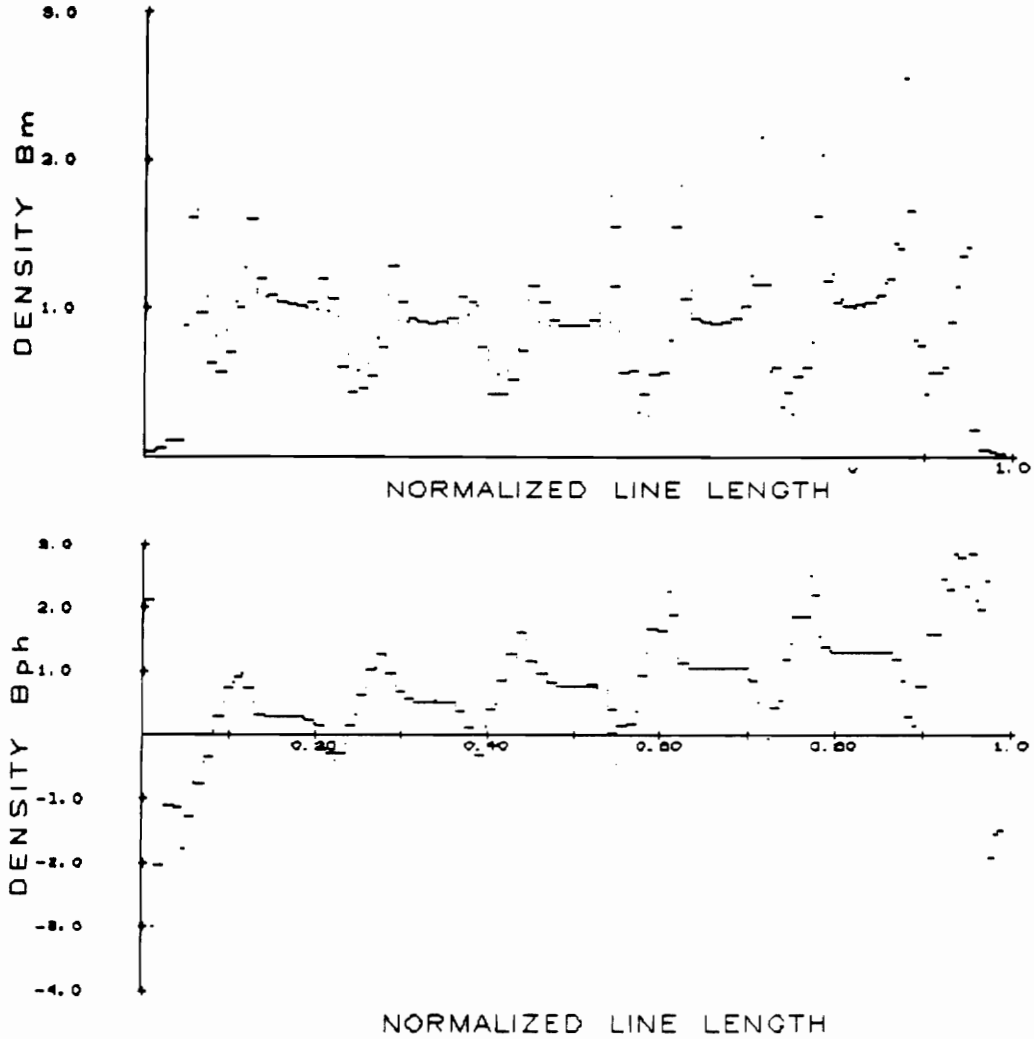

Figure 18. Flux Density in Air-gap of the Permanent Magnet Machine

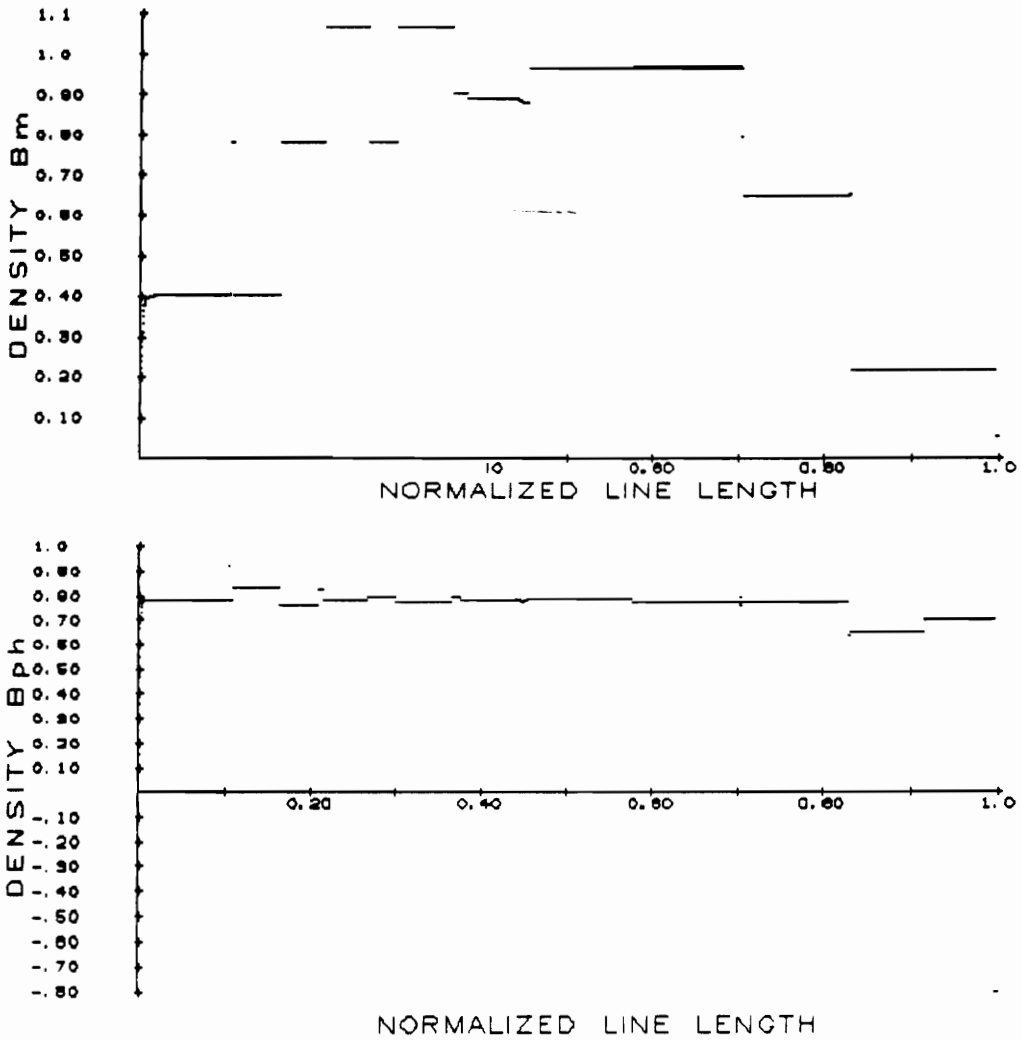

Figure 19. Flux Density along the radius of the Permanent Magnet Machine

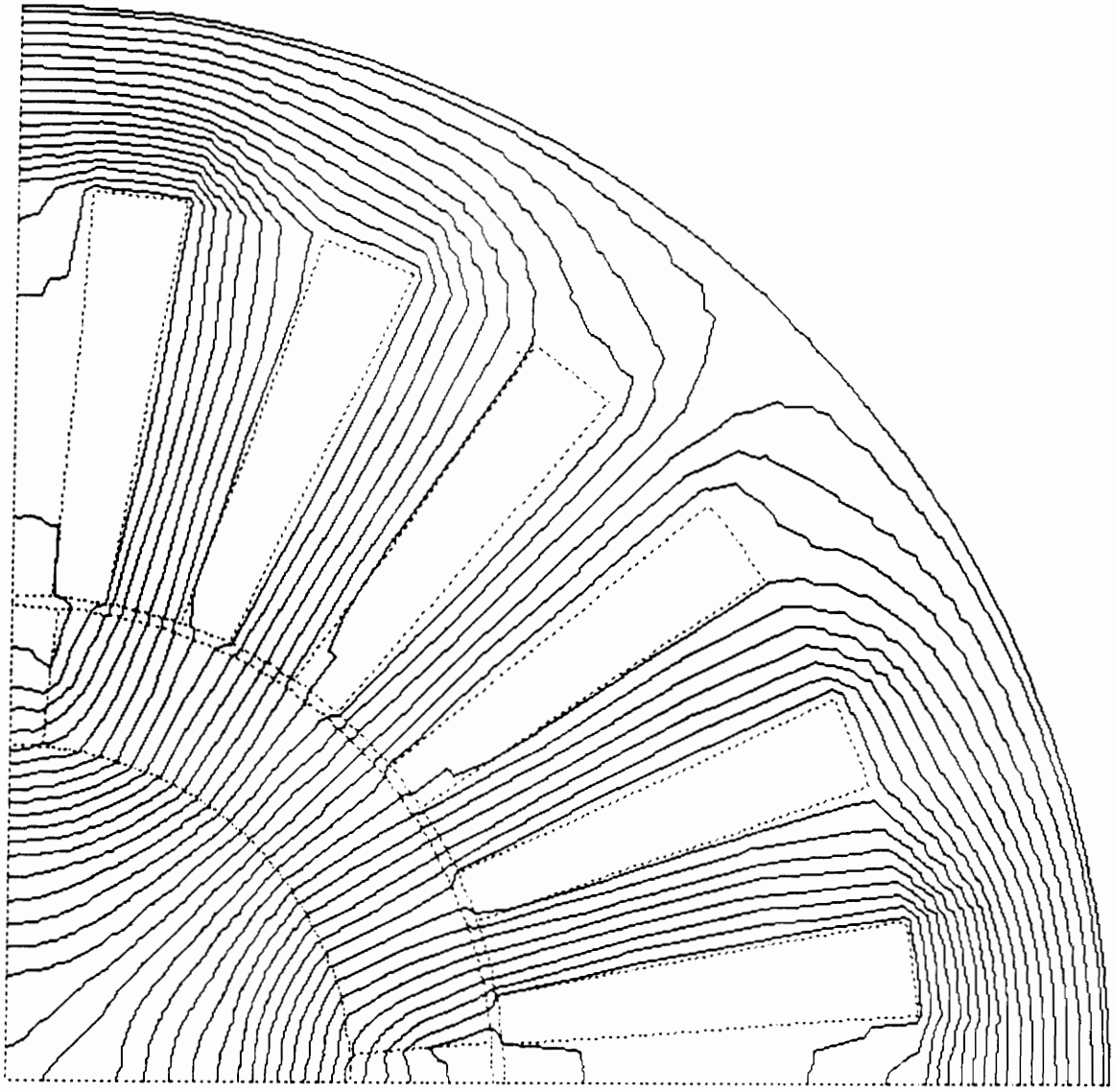

Figure 20. No-load Flux Density in the Permanent Magnet Machine

R_a, R_b, R_c, and R_f are the resistances of phases A, B, C, and the field respectively.

L_{aa}, L_{bb}, etc are the self inductances.

L_{ab}, L_{ab}, etc are the mutual inductances, and

p is $\frac{d}{dt}$

The rotor being made of stainless steel laminations has a very large resistance. The permanent magnets also have a very high resistance, hence the current induced in the field of a permanent magnet machine will be negligible. Magnequench, the permanent magnet material used in the design of the machine has a large coercivity (10.4 KOe), thus, the flux in the magnetic circuit of the machine can be assumed to be constant. Hence the effect of the three stator currents on the rotor is negligible. Hence the machine model can be further simplified as:

$$\begin{bmatrix} v_a \\ v_b \\ v_c \end{bmatrix} = \begin{bmatrix} R_a & 0 & 0 \\ 0 & R_b & 0 \\ 0 & 0 & R_c \end{bmatrix} \begin{bmatrix} i_a \\ i_b \\ i_c \end{bmatrix} + p \begin{bmatrix} L_{aa} & L_{ab} & L_{ac} \\ L_{ba} & L_{bb} & L_{bc} \\ L_{ca} & L_{cb} & L_{cc} \end{bmatrix} \begin{bmatrix} i_a \\ i_b \\ i_c \end{bmatrix} \qquad [4.2]$$

Assume the three stator windings to be similar in all aspects. That is:

$$L_{ab} = L_{ba} = L_{ac} = L_{ca} = L_{bc} = L_{cb} = M$$

and,

$$L_{aa} = L_{bb} = L_{cc} = L$$

the equation [4.2] can be further simplified as:

$$\begin{bmatrix} v_a \\ v_b \\ v_c \end{bmatrix} = \begin{bmatrix} R & 0 & 0 \\ 0 & R & 0 \\ 0 & 0 & R \end{bmatrix} + p \begin{bmatrix} L-M & 0 & 0 \\ 0 & L-M & 0 \\ 0 & 0 & L-M \end{bmatrix} \begin{bmatrix} i_a \\ i_b \\ i_c \end{bmatrix} \qquad [4.3]$$

The equation [4.3] gives the model of the permanent magnet motor used in the simulation of the inverter-machine model in the latter part of this chapter. Figure 21 on page 62 represents the equivalent circuit of the permanent magnet machine. The machine can be represented by a three phase wye connected winding having a resistance equal to the phase resistance in series with an inductance equal to the leakage inductance in series with a voltage source equal to the induced EMF of the machine.

Simulation of the Machine - Inverter Model

The machine-inverter model is simulated (as explained in Chapter I) using the following methods: (1) SPICE; (2) Analytical program

1. SPICE

2. Analytical program developed.

EQUIVALENT MODEL OF THE PMSM

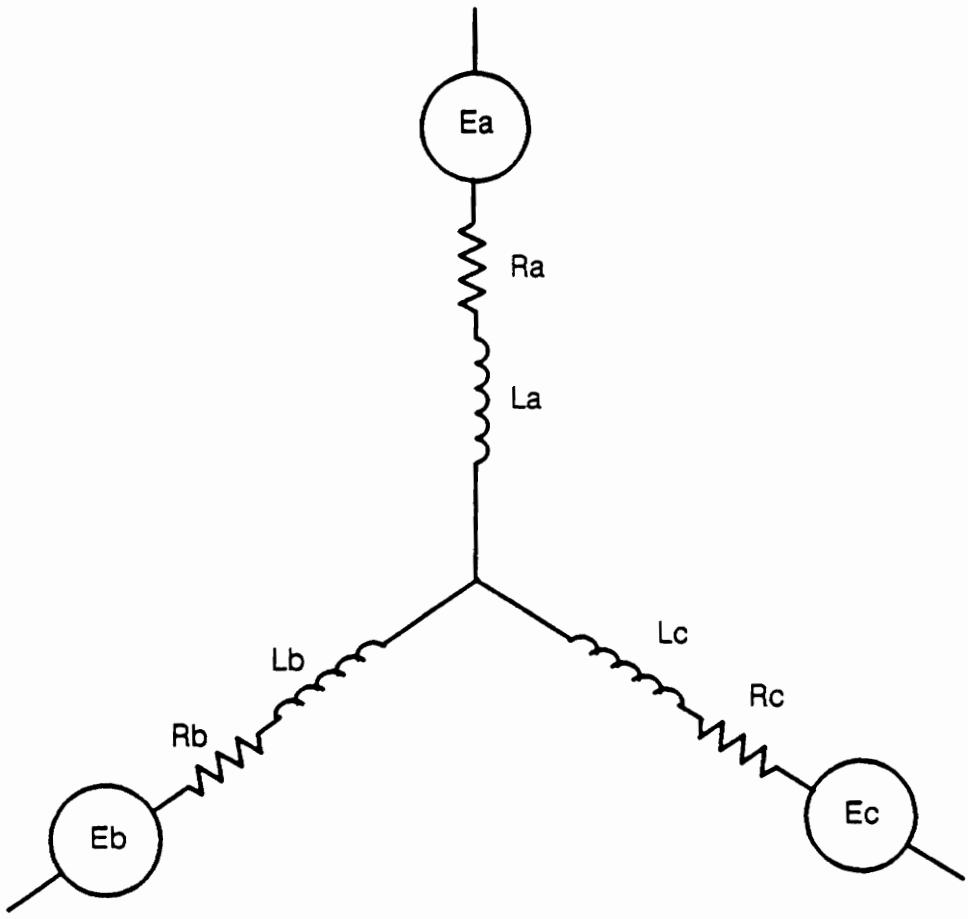

Figure 21. Equivalent Circuit of the Permanent Magnet Machine

Simulation by SPICE

Simulation Program, Integrated Circuit Emphasis (SPICE), is a computer-aided (CAD) tool. SPICE can perform non-linear DC, large-signal time domain (transient), small signal frequency domain and other types of simulation.

The inputs to SPICE are a listing of all the circuit elements, their parameter values, and all the connections. The output is user specified.

Figure 16 on page 50 gives the complete inverter-machine circuit used in the simulation. The transistor model used by SPICE is the Elbers-Moll model (SPICE reference book). The transistor modelled are the MT6006. The free-wheeling diodes are modelled to carry the maximum armature current continuously, and are rated equal to the maximum continuous current of the transistor. The snubber capacitance and resistance are calculated as explained in Chapter III. The simulation is done for 8 ms and Figure 22 on page 64 gives the current in phase A.

Simulation using the Analytical Program

The analytical program was developed to simulate the inverter-machine model. This program was based on the different modes of operation in one operation cycle (Figure 23 on page 66). The machine is modelled as explained in the previous section. The switches are modelled as non-linear resistances. The free-wheeling diodes are modelled as resistances in series with a constant voltage source when the device is on, and as open circuit when it is off. The snubber circuit is not modelled. The transistors are

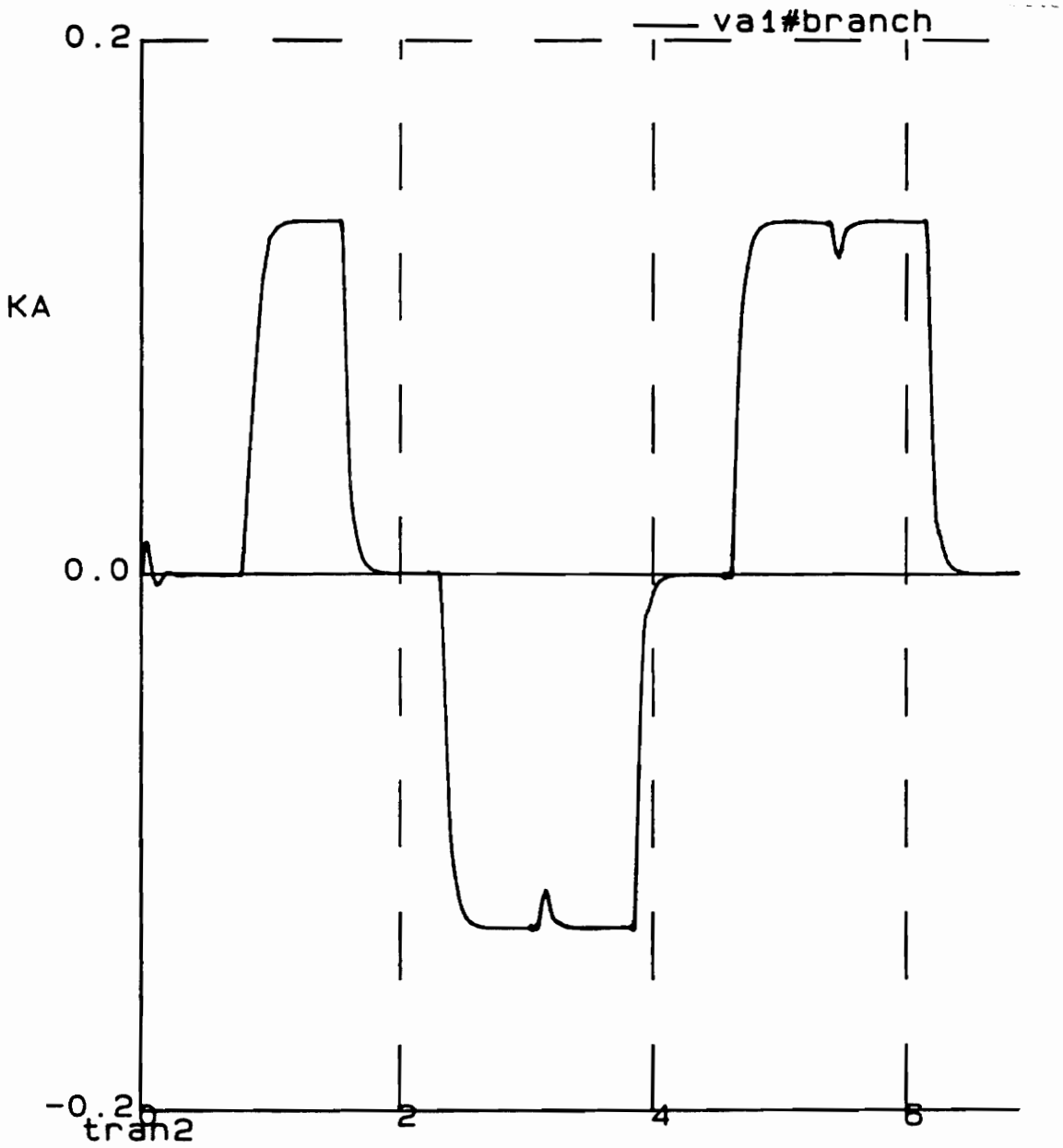

Figure 22. Current in Phase A – SPICE Simulation

assumed to be ideal, i.e. there are no fall-times and rise-times. Hence, the snubber circuits can be eliminated. During the on-cycle each transistor is switched on for a total period of 120. The switching sequence in one cycle or 360 is:

0 - 60 degrees	Tr6, Tr1 on	rest off
60 - 120 degrees	Tr1, Tr2 on	rest off
120 - 180 degrees	Tr2, Tr3 on	rest off
180 - 240 degrees	Tr3, Tr4 on	rest off
240 - 300 degrees	Tr4, Tr5 on	rest off
300 - 360 degrees	Tr5, Tr6 on	rest off

To take into consideration the rise time and the fall-time of the transistors, it is assumed that each mode of operation is a little less than 60 degrees. The respective free-wheeling diode conducting during that time. Hence, the analytical program assumes that in one cycle there are 12 modes of operation:

Mode 1	Tr 6 - Tr 1	0 - < 60 degrees
Mode 2	Tr 1 - FD 6	< 60 - 60 degrees
Mode 3	Tr 1 - Tr 2	60 - < 120 degrees
Mode 4	Tr 2 - FD 1	< 120 - 120 degrees
Mode 5	Tr 2 - Tr 3	120 - < 180 degrees
Mode 6	Tr 3 - FD 2	< 180 - 180 degrees
Mode 7	Tr 3 - Tr 4	180 - < 240 degrees
Mode 8	Tr 4 - FD 3	< 240 - 240 degrees
Mode 9	Tr 4 - Tr 5	240 - < 300 degrees
Mode 10	Tr 5 - FD 4	< 300 - 300 degrees
Mode 11	Tr 5 - Tr 6	300 - < 360 degrees
Mode 12	Tr 6 - FD 5	< 360 - 360 degrees

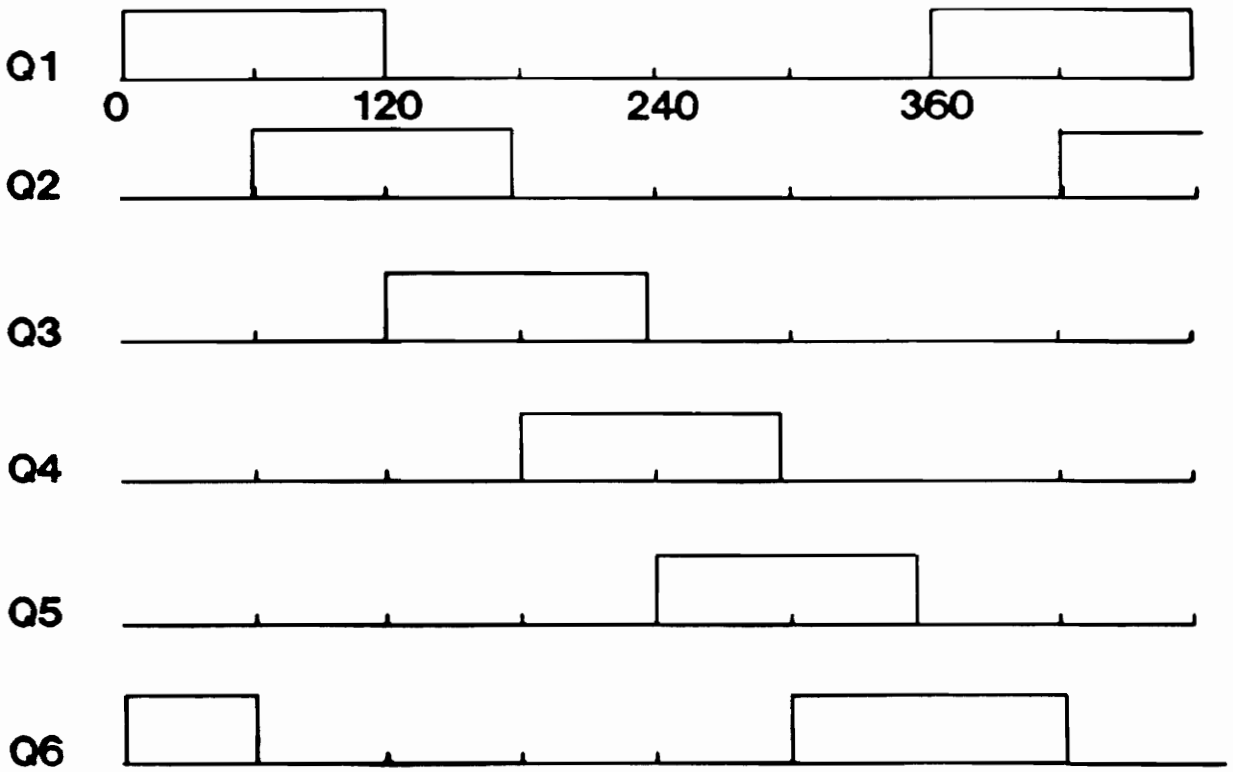

Figure 23. Firing Sequence of the Inverter

Twelve different subroutines were developed based on the conditions in each mode. The equivalent circuit for mode one shown in Figure 24 on page 68. The differential equation governing mode one is:

$$V_{dc} = (R_a + R_b + R_{t1} + R_{t6})\, i + (L_a + L_b)\, \frac{di}{dt} + E_a - E_b \qquad [4.4]$$

The initial conditions are assumed to be 0.0. The differential equations governing mode two (Figure 25 on page 69) are:

$$(R_a + R_b + R_{t1} + R_d)\, i + (L_a + L_b)\, \frac{di}{dt} + E_a - E_b + E_d = 0 \qquad [4.5]$$

The initial conditions are obtained from the earlier subroutine. The differential equations governing mode 3 (Figure 26 on page 70) are:

$$V_{dc} = (R_a + R_c + R_{t1} + R_{t2})\, i + (L_a + L_c)\, \frac{di}{dt} + E_a - E_c \qquad [4.6]$$

and the initial conditions are obtained from the previous subroutine. Similarly, the differential equations for the following nodes are:

Mode 4 (Figure 27 on page 71) :

$$(R_a + R_c + R_{t2} + R_{d1})\, i + (L_a + L_c)\, \frac{di}{dt} + E_a - E_c + E_d = 0 \qquad [4.7]$$

Mode 5 (Figure 28 on page 72) :

$$V_{dc} = (R_b + R_c + R_{t2} + R_{t3})\, i + (L_b + L_c)\, \frac{di}{dt} + E_b - E_c \qquad [4.8]$$

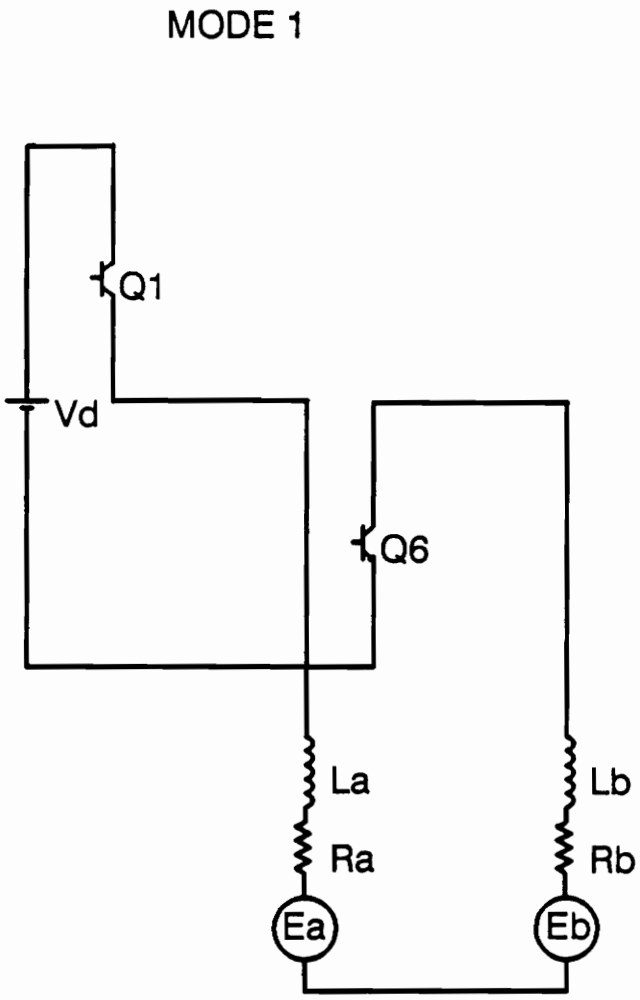

Figure 24. Machine- Inverter Circuit - Mode 1

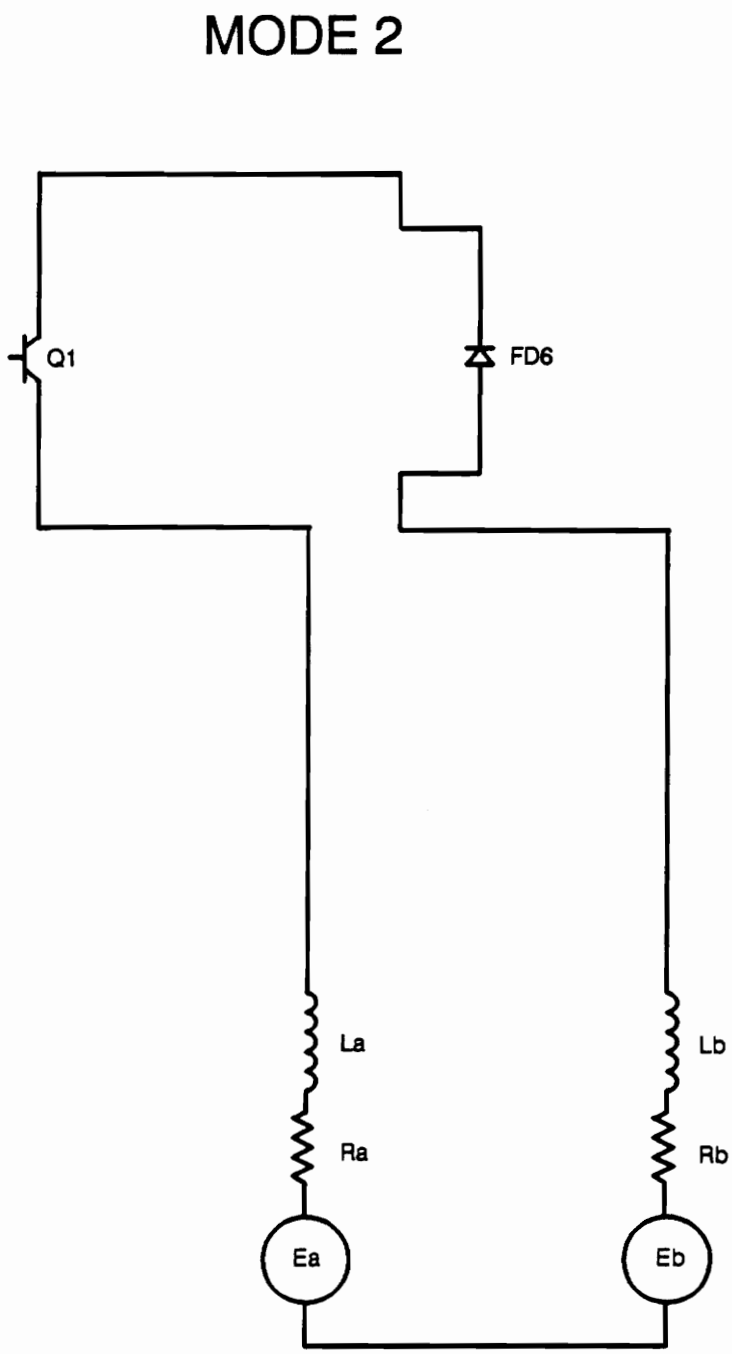

Figure 25. Machine- Inverter Circuit - Mode 2

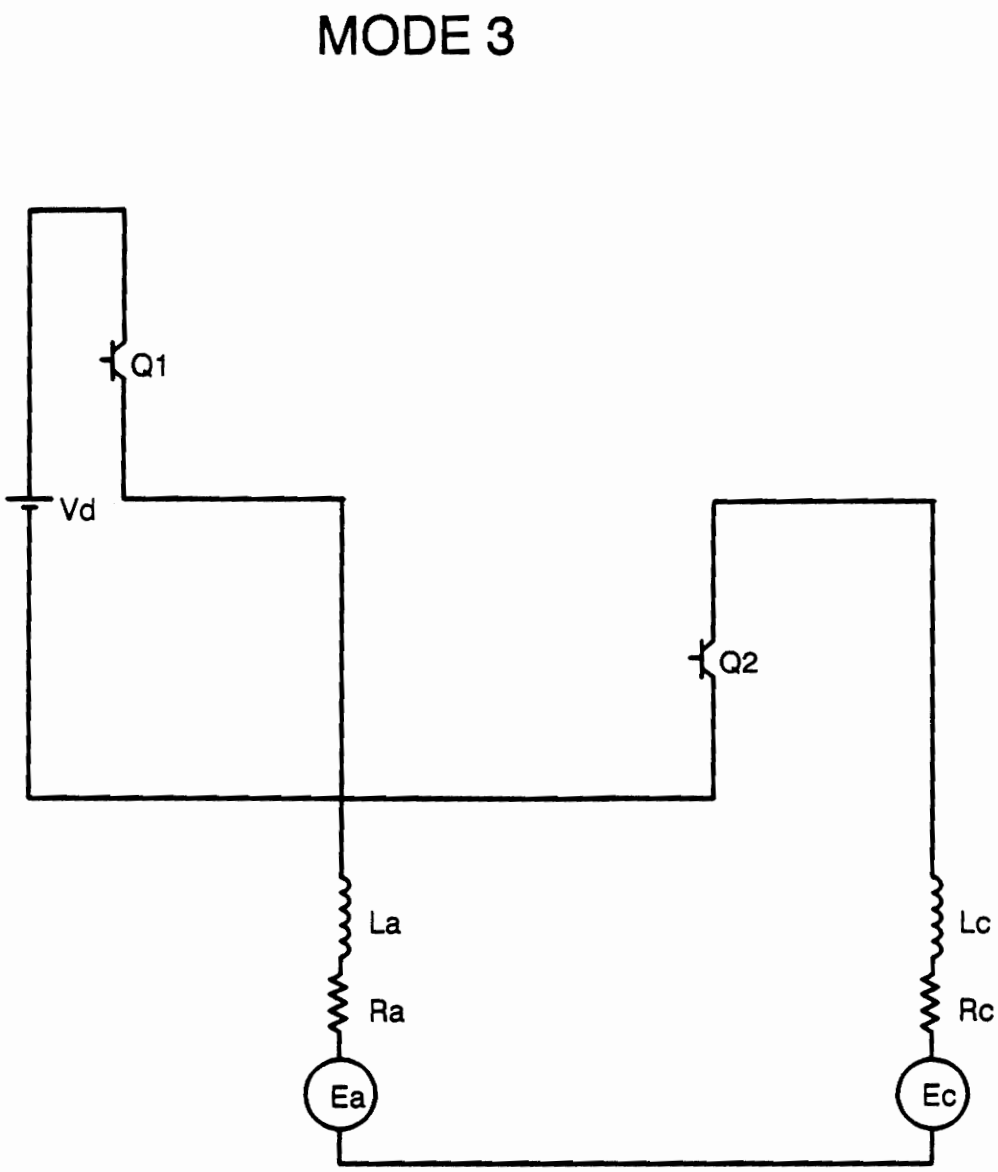

Figure 26. Machine- Inverter Circuit - Mode 3

MODE 4

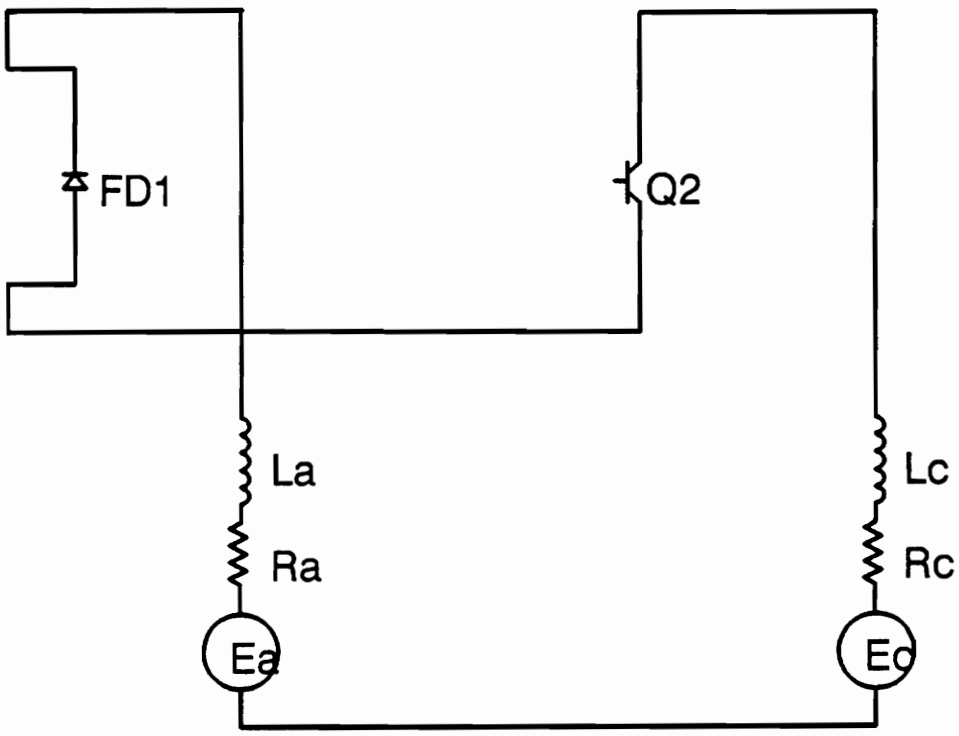

Figure 27. Machine- Inverter Circuit - Mode 4

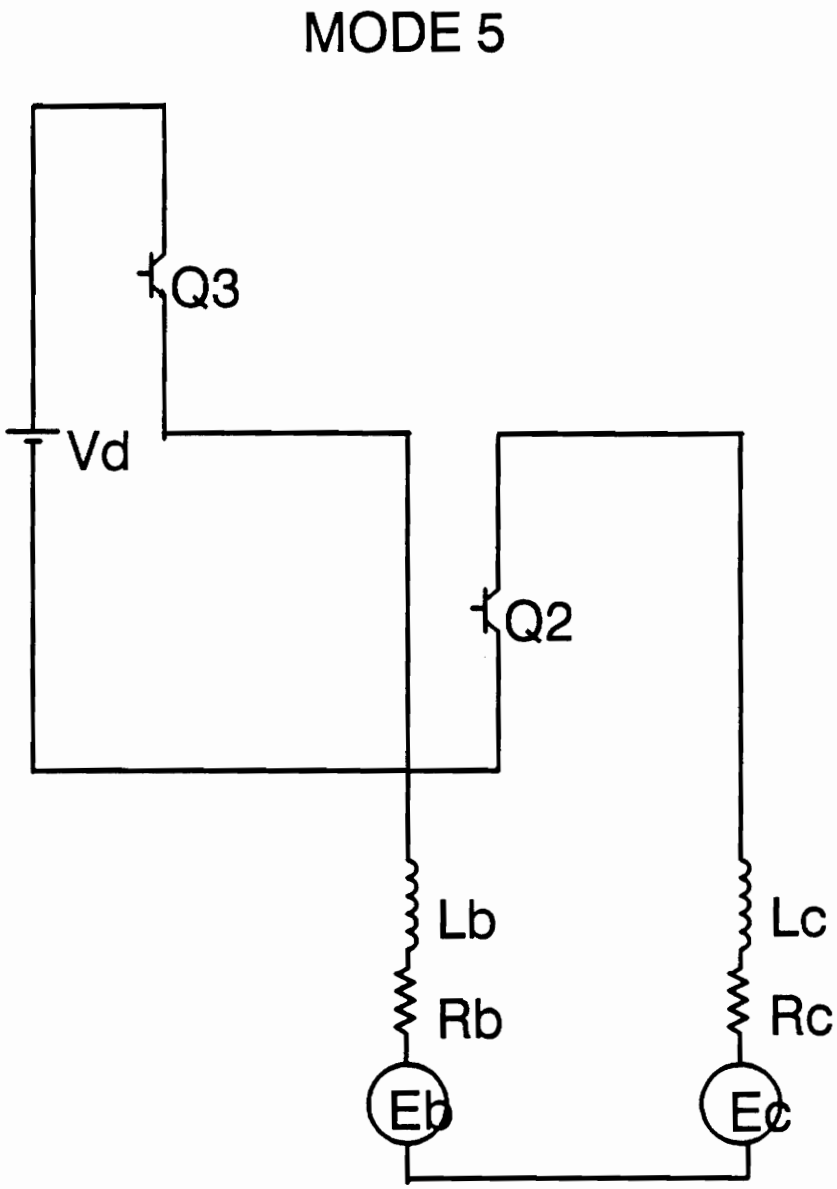

Figure 28. Machine- Inverter Circuit - Mode 5

Mode 6 (Figure 29 on page 74) :

$$(R_b + R_c + R_{t3} + R_{d2})\, i + (L_b + L_c)\, \frac{di}{dt} + E_b - E_c + E_d = 0 \qquad [4.9]$$

Mode 7 (Figure 30 on page 75) :

$$V_{dc} = (R_b + R_a + R_{t3} + R_{t4})\, i + (L_b + L_a)\, \frac{di}{dt} + E_b - E_a \qquad [4.10]$$

Mode 8 (Figure 31 on page 76) :

$$(R_b + R_a + R_{t4} + R_{d3})\, i + (L_b + L_a)\, \frac{di}{dt} + E_b - E_a + E_d = 0 \qquad [4.11]$$

Mode 9 (Figure 32 on page 77) :

$$V_{dc} = (R_c + R_a + R_{t4} + R_{t5})\, i + (L_c + L_a)\, \frac{di}{dt} + E_c - E_a \qquad [4.12]$$

Mode 10 (Figure 33 on page 78) :

$$(R_c + R_a + R_{t5} + R_{d4})\, i + (L_c + L_a)\, \frac{di}{dt} + E_c - E_a + E_d = 0 \qquad [4.13]$$

Mode 11 (Figure 34 on page 79) :

$$V_{dc} = (R_c + R_b + R_{t5} + R_{t6})\, i + (L_c + L_b)\, \frac{di}{dt} + E_c - E_b \qquad [4.14]$$

Mode 12 (Figure 35 on page 80) :

$$(R_c + R_b + R_{t6} + R_{d5})\, i + (L_c + L_b)\, \frac{di}{dt} + E_c - E_b + E_d = 0 \qquad [4.15]$$

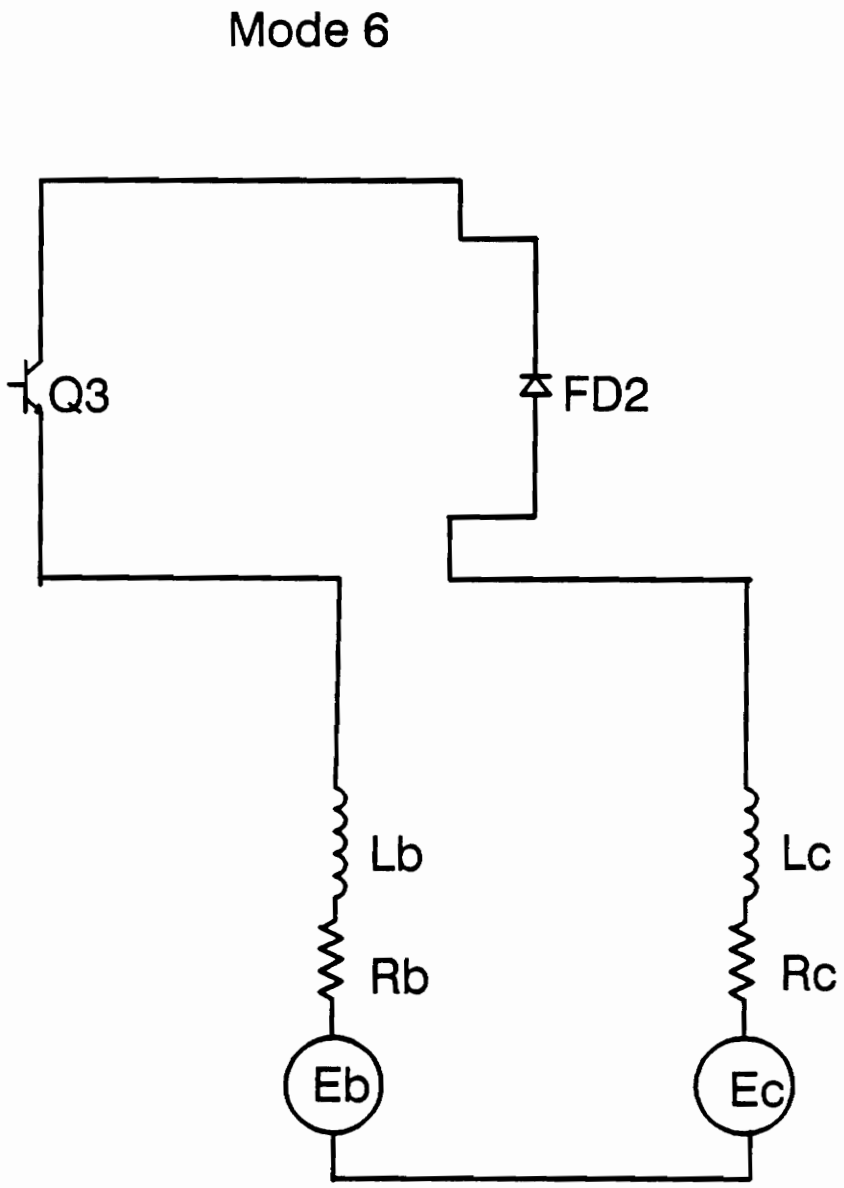

Figure 29. Machine- Inverter Circuit - Mode 6

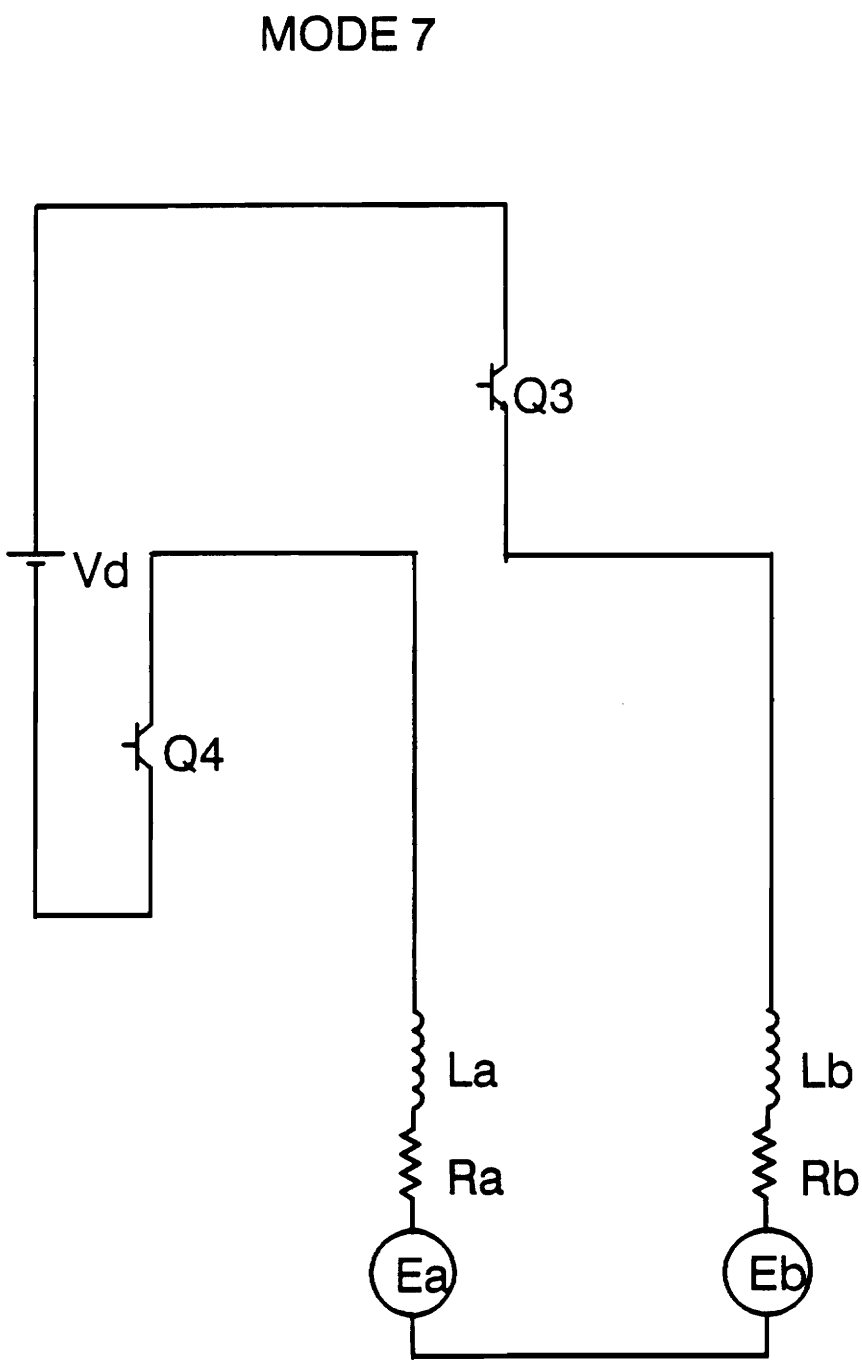

Figure 30. Machine- Inverter Circuit - Mode 7

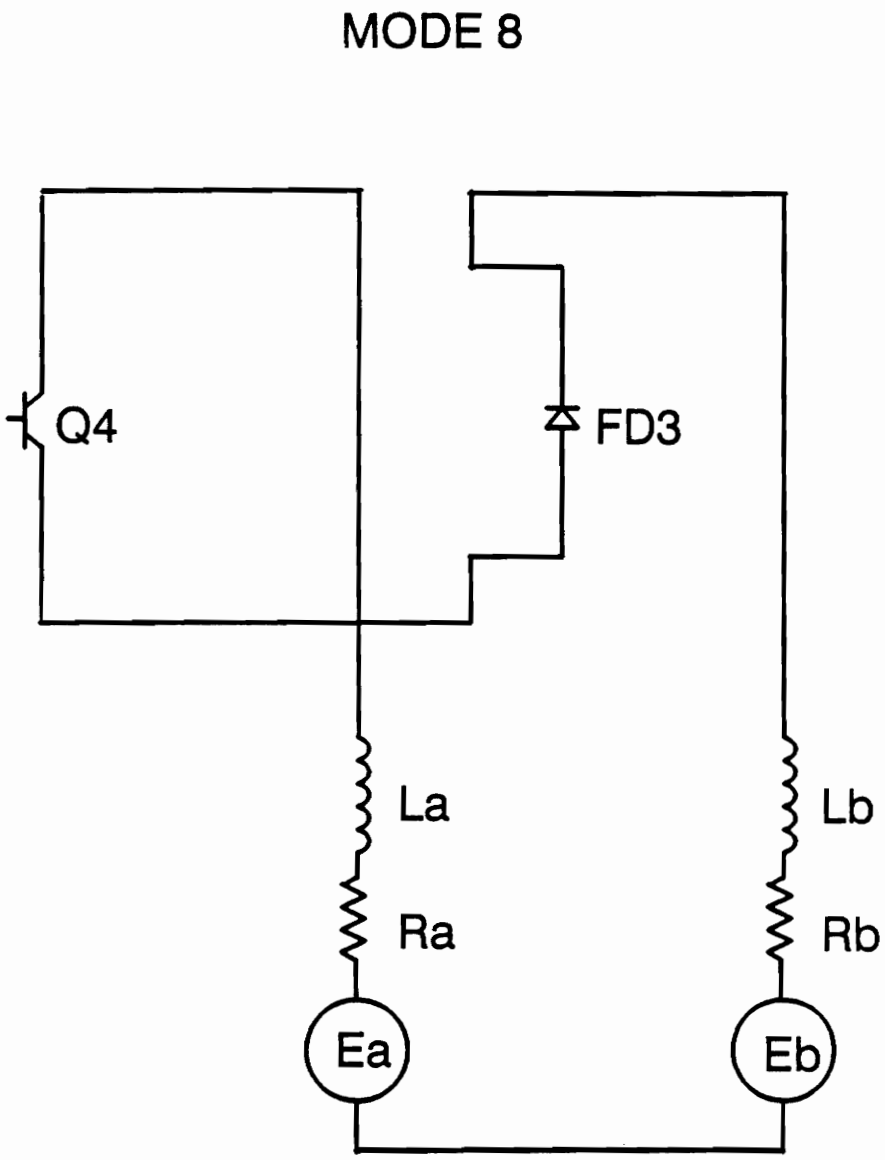

Figure 31. Machine- Inverter Circuit - Mode 8

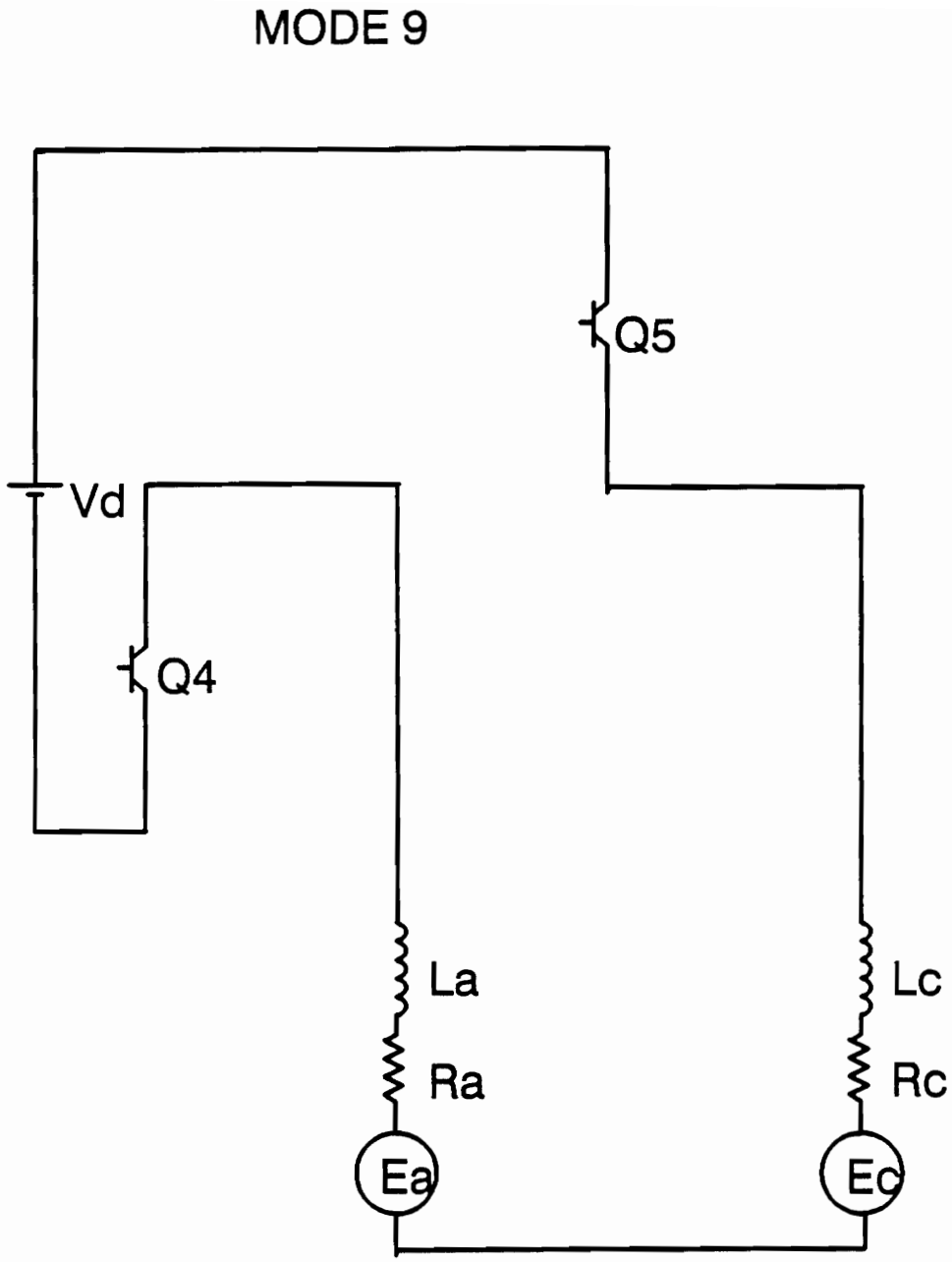

Figure 32. Machine- Inverter Circuit - Mode 9

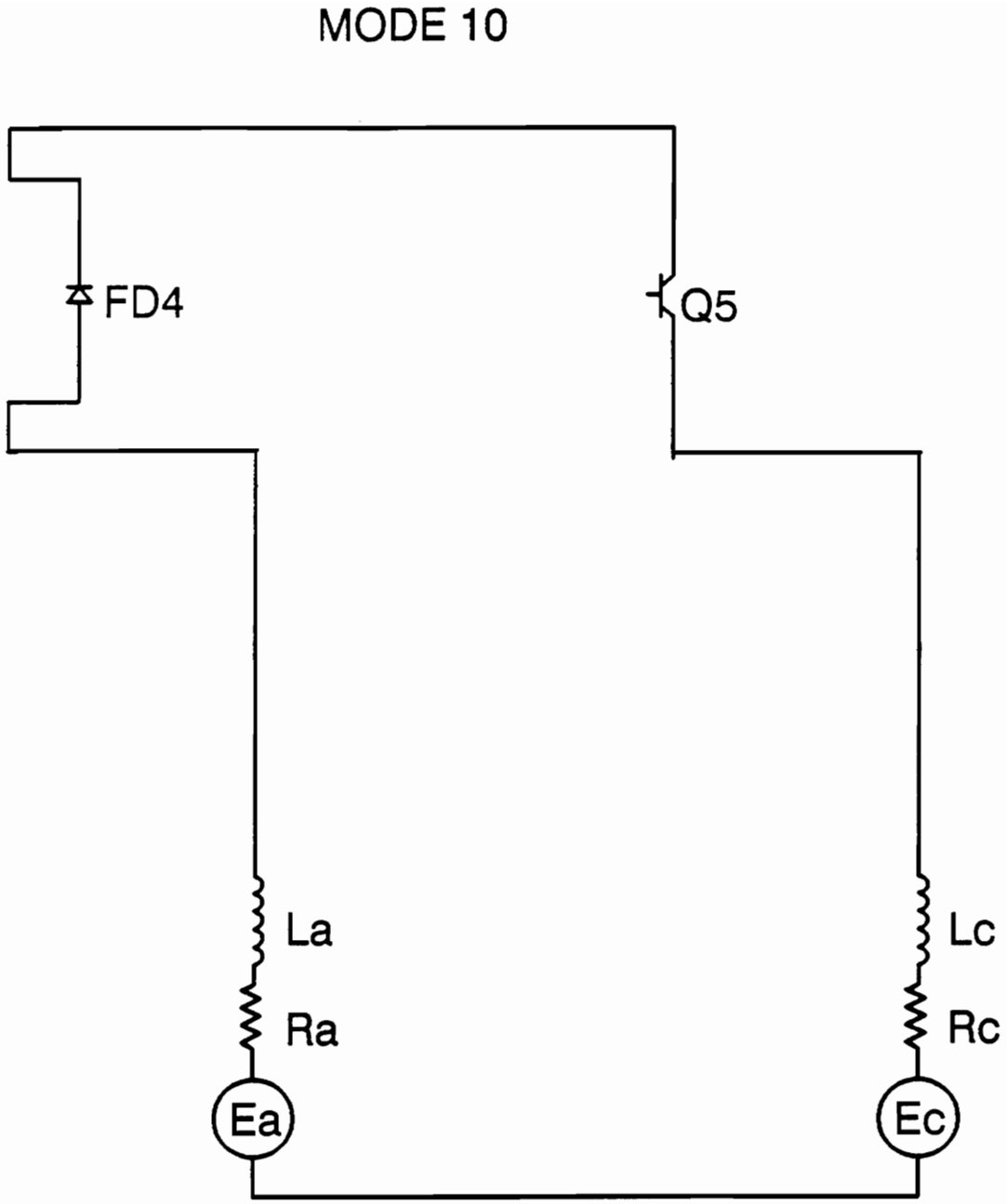

Figure 33. Machine- Inverter Circuit - Mode 10

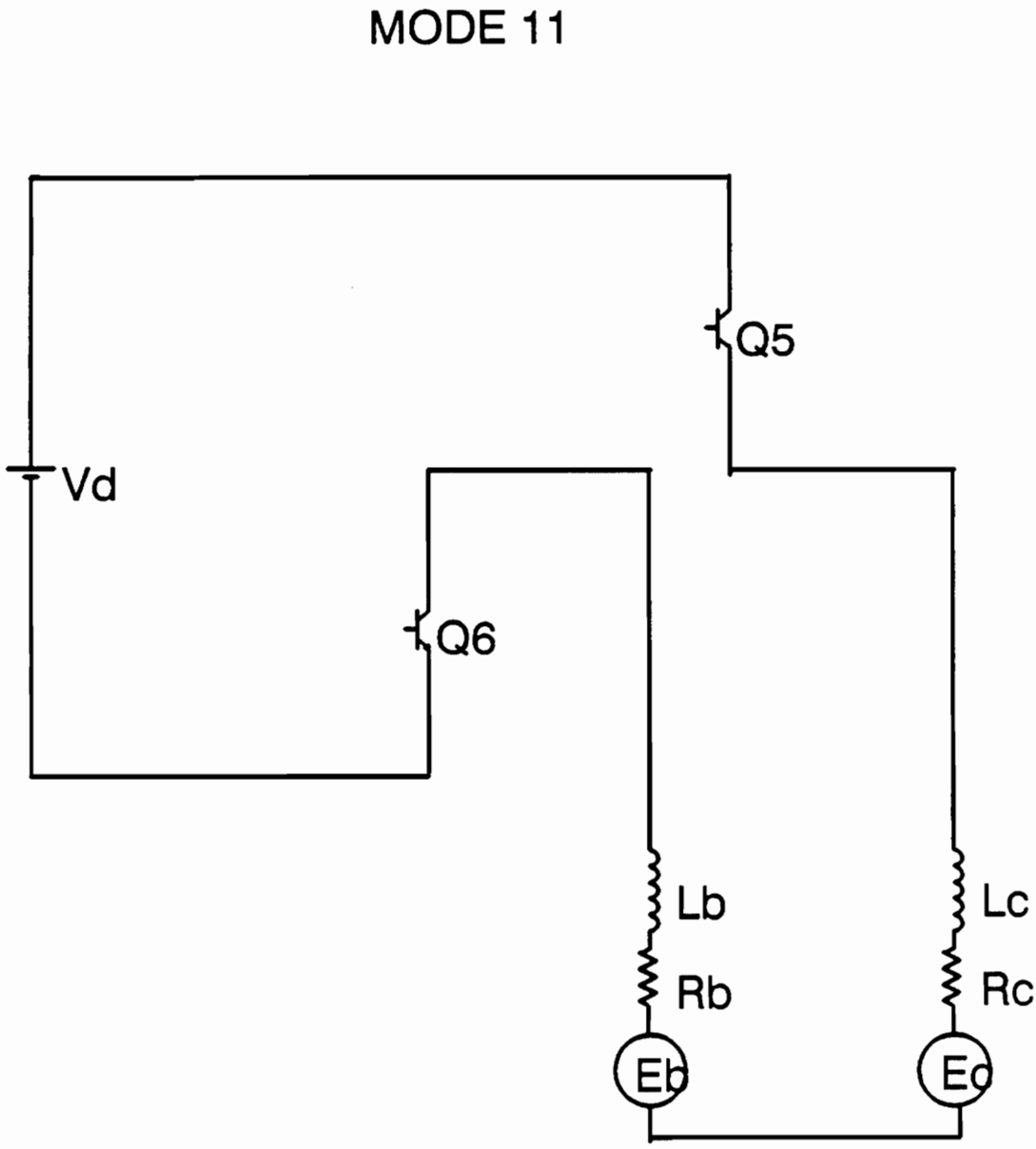

Figure 34. Machine- Inverter Circuit - Mode 11

MODE 12

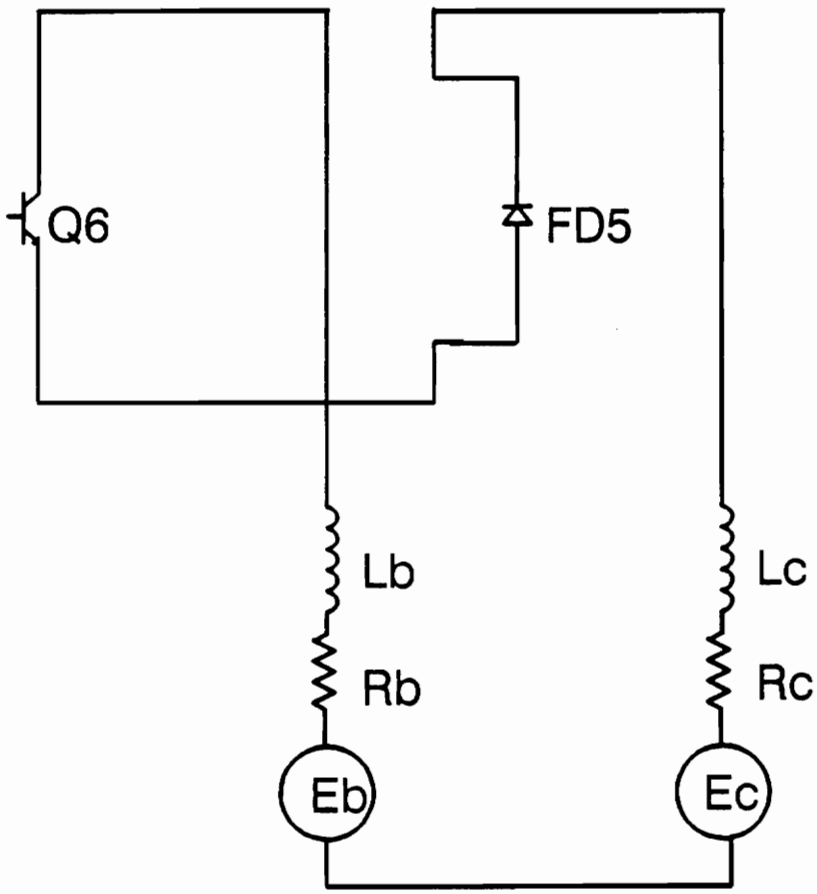

Figure 35. Machine- Inverter Circuit - Mode 12

The back emf is calculated based on the equation :

$$E = n \phi \qquad [4.16]$$

The resistance per phase and the inductance of the machine are calculated based on the procedure outlined in Chapter II. Figure 36 on page 82 show the plot of the current in phase A of the machine against time.

The waveforms are simulated by SPICE and the analytical program are quite similar. There are a few differences in the waveforms. This can be explained as follows. The fall-time of the switch in the analytical program is assumed to be zero. Hence, the current in phase A (Figure 36 on page 82) falls to zero instantaneously. In SPICE, the transistor has a finite fall-time and the current drops to zero in a finite time. Also, in the analytical program the transistor model is simplified to a non-linear resistance unlike the SPICE, in which the transistor is modelled by the more complicated Elber-Moll model.

The analytical model calculates the back EMF, and uses this as input, whereas in the SPICE simulation the back EMF should be supplied as an input and is fixed quantity. Hence, the SPICE simulation is done of full-speed conditions, unlike the analytical program which can simulate for varying conditions.

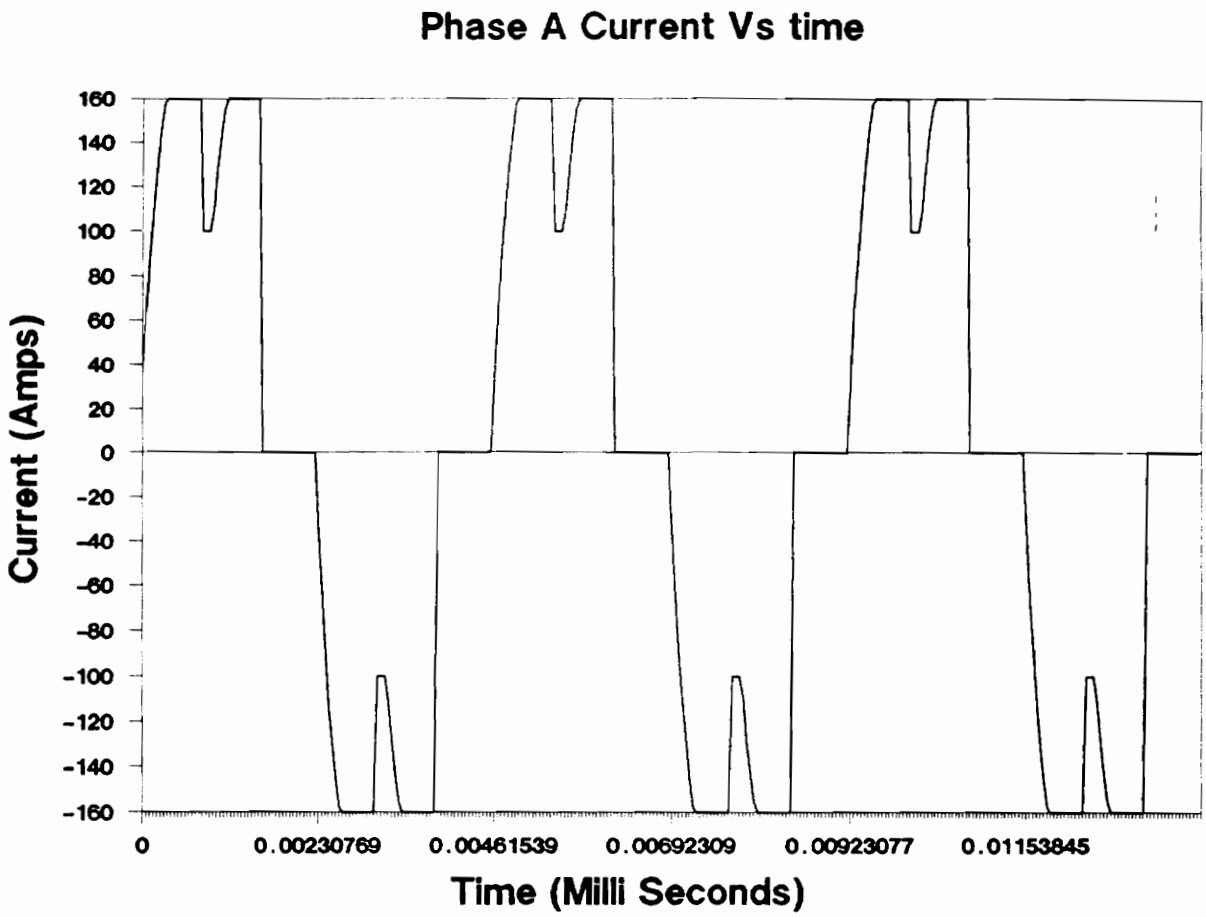

Figure 36. Current in Phase A – Analytical Program

Conclusions

In this thesis a permanent magnet machine and drive, for cranking purposes, were successfully designed. Based on the constraints set by the problem, a new procedure was developed. The design procedure developed is superior to the conventional design procedure because it takes the current density in A/mm^2 into consideration unlike the conventional design procedures which are based on the current loading in A/mm The developed procedure is superior as it takes the actual current flowing in the conductors, and hence the thermal constraints can be incorporated from the beginning of the design procedure. The main assumptions made in the design approach were verified using a standard Finite Element Method, WEMAP, and another analytical program developed by De La Ree and Boules.

The drive was designed and simulated by two methods, SPICE and an analytical program developed as a part of this thesis. The drive could not be experimentally verified because of the constraints on the maximum current that can be tested in the laboratory. Hence, the machine - inverter model was simulated successfully using the standard CAD package SPICE, and an analytical program.

A permanent magnet brushless machine having an outer diameter of 10 cm., a rotor length 0f 2.5 cm., and capable of meeting the following three constraints has been designed.

li. Full - load speed of 6500 RPM.

Maximum current density of $35A/mm^2$

Withstand a demagnetizing current of 250 % at 20 C.

Appendix A. Symbols used in the thesis

S = Output in Horse Power

B_g = Average flux density in air-gap

B_t = Maximum flux density in the teeth

B_c = Maximum flux density in the yoke

B_r = Remanent flux density

J = Current density

E = Induced EMF per phase

D_{si} = Inside diameter of the stator

D_{so} = Outside diameter of the stator

L = Axial length of the machine

τ_p = Pole pitch

τ_s = Slot pitch

α_p = Pole pitch

L = Axial length of the rotor

b_t = Tooth width

h_t = Tooth height

b_i = Width of yoke or back iron

h_m = Height of magnet

δ = Length of air-gap

N_s = Number of slots

T_{ph} = Number of turns per phase

d_{cu} = Diameter of copper conductor

A_s = Area of slot

A_{cu} = Area of copper in slot

p = Number of pole pairs

m = Number of phases

f = Frequency

n = Speed in rps

K_f = Form factor

K_w = Winding factor

K_{cu} = Copper filling factor

K_d = Distribution factor

K_c = Carter Coefficient

K_{sa} = Saturation factor

Appendix B. Main dimensions and parameters of the Cranking Motor.

Remanent flux density of Magnaquench	1.2	Tesla
Flux densty in air-gap	0.96	Tesla
Maximum flux densty in teeth	1.6	Tesla
Maximum flux densty in yoke	1.2	Tesla
Number of pole pairs	2	
Pole pitch	85.5	degrees
Stator outside diameter	100	mm
Stator inside diameter	45.0	mm
Rotor outside diameter	30.0	mm
Core length	2.5	~~mm~~ cm
Magnet height	6.5	mm
Stator back-iron thickness	8.5	mm
Stator slot height	19	mm
Airgap length	1.0	mm

Pole pitch	35.2	mm
Slot pitch	5.90	mm
Number of turns per phase	8	
Supply voltage	12	V
Rated peak current	165	A
Core Material		Steel
Rated speed	6500	r.p.m.
Wire gauge	AWG 11	

References

1. N. Boules "Two-Dimensional Field Analysis of Cylindrical Machines with Permanent Magnet Excitation," *Conf.Rec 1983 IEEE Ind.Appl.Soc.Ann.Mtg.*, pp 446-454.

2. N. Boules "Design Optimization of Permanent Magnet DC Motors," *Conf.Rec. 1987 IEEE Ind.Appl.Soc.Ann.Mtg.*, pp 27-33.

3. R.S. Colby "Classification of Inverter Driven Permanent Magnet Synchronous Motors," *Conf.Rec 1988 IEEE Ind.Appl.Soc.Ann.Mtg.*, pp 1-6.

4. B. Davat, H. Rrezine, and M. Lajoie-Mazenc "Eddy Currents in Solid Rotor Permanent Magnet Synchronous Motors fed by voltage Inverter," *Electric Machines & Electromagnetics*, vol 7, pp 115-124, 1982.

5. J. De La Ree, and N. Boules "Torque Production in Permanent Magnet Synchronous Motors," *Conf.Rec. 1987 IEEE Ind.Appl.Soc.Ann.Mtg.*, pp 15-20.

6. J. De LA Ree, and J. Latorre "Permanent Magnet Machines Torque Considerations," *Conf.Rec. 1988 IEEE Ind.Appl.Soc.Ann.Mtg.*, pp 32-37.

7. D.M. Erdman, H.B. Harms, J.L. Oldenkamp "Electronically Commutated DC Machines for the Appliance Industry," *Conf.Rec. 1984 IEEE Ind.Appl.Soc.Ann.Mtg.*, pp 1339-1345.

8. A.V. Gumaste, and G.R. Slemon "Steady state analysis of Permanent Magnet Synchronous Motor Drive with voltage Source Inverter," *Conf.Rec. 1980 IEEE Ind.Appl.Soc.Ann.Mtg.*, pp 618-625.

9. V.B. Honsinger "Sizing Equations for Electrical Machinery" *IEEE Trans Energy Conversion*, vol EC-2, no. 1, pp 116-121, March 1987.

10. T.M. Jahns "Torque Production in Permanent Magnet Synchronous Motor Drives with rectangular Current excitation," *IEEE Trans. Industrial Applications*, vol IA-20, no. 4, pp 803-813, July/August 1984.

11. P.C. Krause, and T.A. Lipo "Analysis and Simplified Representations of a Rectifier-Inverter Induction Motor Drive" *IEEE Trans.Power Apparatus Systems*, vol PAS-88, no. 5, pp 588-596, 1969.

12. E. Levi, "Polyphase Motors," John Whiley & sons, Inc.

13. T.A. Lipo, F.G. Turnbull "Analysis and Comparison of Two Types of Square Wave Inverter Drives" *IEEE Trans. Industrial Applications*, vol IA-11, no. 2, pp 137-147.

14. T.A. Lipo "The Analysis of Induction Motors with voltage Control by Symmetrically Triggered Thyristors," *IEEE Trans. Power Apparatus Systems*, vol PAS-90, no. 2, pp 515-525, 1971.

15. T. Nehl, F. Fouad, and N. Dermerdash "Dynamic Simulation of Radially-Oriented Permanent Magnet Type Electronically Operated Synchronous Machines with Parameters obtained from Finite Element Field Solutions," *IEEE Trans. Industrial Applications*, vol IA-18, no. 2, pp 172-182, March/April 1982.

16. T.W. Nehl "A Discrete Time Model of a Power Conditioner fed Permanent Magnet Brushless DC Motor Systems," Ph. D. Thesis, VPI&SU, 1980.

17. D.W. Novatny, and F.A. Fath "The Analysis of Induction Machines Controlled by Series connected Semiconductor Switches," *IEEE Trans. Power Apparatus Systems*, vol PAS-87, no. 2, pp 597-605, 1968.

18. B. Patel *GMRL Report*,

19. G. Pfaff, A. Weschta, and A. Wick "Design and Experimental Results of a Brushless AC Servo Drive," *Conf.Rec. 1982 IEEE Ind.Appl.Soc.Ann.Mtg.*, pp 692-697.

20. P. Pillay "Modeling, Simulation, and Analysis of Permanent Magnet Synchronous and Brushless DC Motor Systems," Ph. D. Thesis, VPI&SU, 1987.

21. T. Sebastian, and G.R. Slemon "Design Considerations for Variable Speed Permanent Magnet Motors" *Proc. Intl.Conf. on Electric Machines*, pp 1099-1102, 1986.

22. G.R. Slemon, and A.V. Gumaste "Steady State Analysis of a Permanent Magnet Synchronous Motor Drive with Current Source Inverter," *Conf.Rec. 1981 IEEE Ind.Appl.Soc.Ann.Mtg.*, pp 683-690.

23. G.R. Slemon "Analytical Models for saturated Synchronous Machines", *IEEE Trans. Power apparatus Systems*, vol PAS-90, no.2, pp 409-417, March/April 1971.

24. A. Weschta "Design Considerations and Performance of Brushless Permanent Magnet Servo Motors," *Conf.Rec. 1982 IEEE Ind.Appl.Soc.Ann.Mtg.*, pp 469-475.

25. W. McMurry "Selection of Snubbers and Clamps to Optimize the Design of Transistor Switching Converters," *IEEE Trans. Industry Applications*, vol IA-16, no.4, pp 513-523, July/August 1980.

26. E.T. Calkin, and B.H. Hamilton "Circuit Techniques for Improving the Switching Loci of Transistor Switches in Switching Regulators," *IEEE Trans. Industry Applications*, vol IA-12, no.4, pp 364-369, July/August 1976.

27. C.G. Steyn, and J.D. Van Wyk "Optimum Non-linear Turn-off Snubbers: Design and Application," *IEE Conf.Publ.264*, pp 469-475, 1986.

28. T. Kenjo, and S. Nagamori "Permanent-Magnet and Brushless DC Motors" *Clarendon Press, Oxford, 1985.*

29. Dr. Krishnan Ramu "Class Notes" *VPI & SU*

Vita

Gita Pappu was born in Visakhapatnam, India on the 22nd of September, 1964. She completed her bachelors in Electrical Engineering from Andhra University in July 1986. She enrolled for a Masters program in Electrical Engineering in Fall 1987 at Virginia Polytechnic Institute and State University and has been there since. She is a student member of the IEEE, and a member of Eta Kappa Nu, the National Electrical and Computer Engineering Honor society.

Gita Pappu

Gita Pappu